

DEVELOPMENT OF MULTIBODY SOFT TISSUE MODELS AND THEIR TUNING TO  
EXPERIMENTAL DATA: WITH A FOCUS ON THE CANINE MENISCUS

A THESIS IN  
Mechanical Engineering

Presented to the Faculty of the University  
of Missouri-Kansas City in partial fulfillment of  
the requirements for the degree

MASTER OF SCIENCE

By  
GAVIN CARSON PAIVA

B.S., University of Missouri-Kansas City, 2008

Kansas City, Missouri

2010

© 2010

GAVIN CARSON PAIVA

ALL RIGHTS RESERVED

DEVELOPMENT OF MULTIBODY SOFT TISSUE MODELS AND THEIR TUNING TO  
EXPERIMENTAL DATA: WITH A FOCUS ON THE CANINE MENISCUS

Gavin Paiva, Candidate for the Master of Science Degree

University of Missouri-Kansas City, 2010

ABSTRACT

This study explores the application of multibody modeling techniques in an attempt to capture the flexible behavior of biological tissues inside of a rigid body mechanics software. To accomplish this, segmented multibody models of canine menisci were created and the parameters governing the interaction of adjacent segments were tuned to create an overall physiological meniscus behavior. To this extent an experiment was designed to determine whole meniscus deformation under a semi-physiological loading. Additionally, indentation testing of articular cartilage of the canine stifle was performed with the intent of calibrating a cartilage multibody model. The meniscus testing included both sinusoidal and linear ramp loading profiles as well as two separate boundary conditions. Design of Experiments was then used to minimize the error in the model relative to the sinusoidal trials and the ramp profiles were used for validation. While the method proved capable of representing the experimental behavior the optimized parameter sets did not correlate with each other as well as expected.

The undersigned, appointed by the Dean of School of Computing and Engineering, have examined the thesis titled "Development of Multibody Soft Tissue Models and Their Tuning to Experimental Data: With a Focus in the Canine Meniscus," presented by Gavin Paiva, candidate for the Master of Science in Mechanical Engineering degree, and certify that in their opinion it is worthy of acceptance.

Supervisory Committee

Trent Guess, Ph.D., Committee Chairperson  
School of Computing and Engineering

Ganesh Thiagarajan, Ph.D  
School of Computing and Engineering

Greg King, Ph.D.  
School of Computing and Engineering

## CONTENTS

|   |      |
|---|------|
| ABSTRACT .....                            | iii  |
| ILLUSTRATIONS .....                       | vi   |
| TABLES .....                              | viii |
| ACKNOWLEDGMENTS .....                     | ix   |
| Chapter                                   |      |
| 1: Introduction .....                     | 1    |
| 1.1 Background of Materials .....         | 2    |
| 2: Literature Review .....                | 4    |
| 3: Methods .....                          | 8    |
| 3.1 Experimental Testing.....             | 8    |
| 3.2 Model Creation .....                  | 13   |
| 3.3 Model Execution .....                 | 22   |
| 3.4 Design of Experiments.....            | 22   |
| 4: Results.....                           | 23   |
| 4.1 Experimental Testing.....             | 23   |
| 4.2 Model Results.....                    | 28   |
| 5: Discussion .....                       | 37   |
| 5.1 Analysis of Experimental Results..... | 37   |
| 5.2 Model Results.....                    | 37   |
| 5.3 Improvements.....                     | 41   |
| 6: Conclusion.....                        | 43   |
| REFERENCE LIST.....                       | 45   |
| VITA .....                                | 65   |

## ILLUSTRATIONS

| Figures  | Page |
|--|------|
| 1. A disarticulated canine stifle. Femur and tibia halves (left) and menisci (right) .....   | 9    |
| 2. A 3D model of the lateral meniscus v-block .....  | 10   |
| 3. Meniscus testing apparatus (left) and cartilage indentation (right). .....  | 11   |
| 4. A schematic sketch of the indentation apparatus (with tibia half).....  | 12   |
| 5. 3D Slicer sample window, showing a sagittal MRI with traces in all three planes .....   | 13   |
| 6. Course geometry for a canine tibia, cartilage and meniscus (incomplete) .....   | 14   |
| 7. Smoothed geometries after post processing in Geomagic Studio. ....  | 15   |
| 8. Post processed geometries intersected onto the MRIs .....   | 15   |
| 9. A photo overlay of the smoothed geometries (meniscus in blue, cartilage in yellow, and tibia in red) and the original sample..... | 15   |
| 10. Multibody meniscus under load.....   | 19   |
| 11. A representative ramp loading profile for 2R.....  | 25   |
| 12. A representative sine loading profile for 2R .....   | 25   |
| 13. A representative ramp loading profile for 11L.....   | 26   |
| 14. A representative sine loading profile for 11L .....  | 26   |
| 15. Graphical example of nonlinear force length behavior.....  | 28   |
| 16. MB meniscus results for 11L Medial–Wide.....   | 32   |
| 17. MB meniscus results for 2R Lateral-Wide .....  | 32   |
| 18. MB meniscus results for 2R Lateral-Narrow.....   | 33   |
| 19. MB meniscus results for 14L Lateral-Narrow .....   | 33   |
| 20. MB meniscus results for 11L Medial–Wide.....   | 34   |
| 21. MB meniscus results for 2R Lateral –Wide.....  | 34   |

|  |    |
|--|----|
| 22. MB meniscus results for 2R Lateral-Narrow .....  | 35 |
| 23. MB meniscus results for 14L Lateral-Narrow ..... | 35 |

## TABLES

| Table  | Page |
|--|------|
| 1. Contact parameters used for meniscus on v-block interaction.....  | 18   |
| 2. List of valid meniscus test data. ....                            | 24   |
| 3. Indentation samples .....   | 27   |
| 4. Optimized parameters and errors for the medial 11L meniscus.....  | 29   |
| 5. Optimized parameters and errors for the lateral 2R meniscus.....  | 29   |
| 6. Optimized parameters and errors for the lateral 2R meniscus.....  | 30   |
| 7. Optimized parameters and errors for the lateral 14L meniscus..... | 30   |
| 8. Summary of errors .....   | 31   |
| 9. Collected parameters values for the MB canine meniscus.....       | 31   |
| 10. RMS errors for models when using nominal parameter values .....  | 31   |
| 11. Cartilage indentation modeled Moduli of Elasticity .....         | 36   |



## ACKNOWLEDGMENTS

There are many people who deserve thanks for supporting me or leading me to accomplish this.

First and foremost I have to thank my Advisor, Dr Trent Guess, for providing this excellent opportunity and dealing with me when my motivation and direction were vague at times. I also would like thank my committee, Dr. Ganesh Thiagarajan and Greg King, Ph.D., for their help and providing some diverse opportunities.

I also want to explicitly thank the other members of the Musculoskeletal Biomechanics Research Laboratory. I could not have done this without working side by side with fellow Masters candidate Leo Olcott. Paul Wilson provided considerable information as my immediate predecessor. Dr. Hongzeng Liu, Katherine Bloemker, and Dr. Antonis Stylianou greatly improved the quality of my work by providing useful information, motivation and generally improving the laboratory environment. Lastly I have to give an enormous thanks to Mohammad Kia a Ph.D. candidate in the lab that has been the sounding board for every goofy idea I've had and the panacea for every problem. I can't count the number of problems he fixed just by making me work out loud.

# CHAPTER 1

## INTRODUCTION

Soft tissues in a synovial joint such as the knee provide load sharing, shock absorption, passive stability, and lubrication all of which are crucial for ensuring lasting joint health. Models which include these soft tissue structures are able to better reproduce joint kinematics, loading, and analyze the impact of damage and pathological joint behavior (Guess et al. 2010). Multibody (MB) mechanical modeling is a useful tool for the analysis of biological systems that offers an effective method for modeling body and limb level motions. This methodology when combined with the rigid body assumption creates a very efficient simulation environment that has no difficulty in handling large displacements. This assumption has two large drawbacks: it introduces errors by not allowing for deformation, and it removes the ability to calculate internal stress and strains. To account for small scale deformation due to contact stress, many multibody modeling software permit the definition of a penalty function while allowing limited interpenetration of object geometries. In biological systems this method can adequately describe the interaction of bone and cartilage contacts but the flexibility of many other soft tissue structures cannot be represented this way. Tissues that fall into this category include the meniscus of the knee, ligaments, and tendons. Previous work has demonstrated that a multibody model of a human meniscus consisting of a segmented geometry connected by 6 axis spring-damper field elements can capture much of the flexible behavior and significant amounts of the meniscus function (Guess et al. 2010). Previously the parameters governing the behavior of the 6 axis field elements were arranged to behave like a transverse isotropic material and the values were determined by using Design of Experiments (DOE) to tune the model's error relative to a finite element (FE) model. This work explores experimental methods for

determining parameters for modeling canine soft tissue and focuses on the field element parameters for canine menisci.

## **1.1 Background of Materials**

The biological soft tissues examined in this work are canine stifle articular tibial cartilage and meniscus both of which are similar to all other mammalian knee tissue (Nigg and Herzog 1999). While the roles of these tissue are fairly well understood modeling is necessary to develop an understanding of the interactions in the joint and the mechanisms that may lead to joint degradation.

The primary role of the meniscus is to improve tibiofemoral joint interaction and to increase contact area between the tibia and femur. Its anatomic and material properties allow it to accomplish this role through several functional mechanisms including: distributing loads to reduce contact pressure, joint stabilization through limited transmission of transverse loads, joint lubrication, and energy dissipation by absorbing shock due to its low relative compressive stiffness and visco/poroelastic behavior (Nigg and Herzog 1999; McCann et al. 2009). The macroscopic shape and behavior of the meniscus is reinforced by the tissue level structure. The wedge shape of the meniscus cross-section means that while under the typical physiological compressive axial load the meniscus experiences radial extrusion and enormous tensile hoop stresses. This loading is supported at the tissue level by type I collagen fibers that are predominately orientated circumferentially (Fithian et al. 1990). This directional sensitivity creates at the macroscopic level the commonly observed anisotropy of the meniscus, for the purpose of this work it will be treated as a transverse isotropic material (Chia and Hull 2008).

Articular cartilage fulfills similar roles in the knee by further reducing contact stress but serves the additional purpose of lubricating the bearing surfaces (Sweigart et al. 2004). While articular cartilage is a significantly firmer tissue than the meniscus it is only a fraction of the

stiffness of bone. When healthy, two articular cartilage surfaces are near frictionless as both surfaces are extremely smooth and exude fluid to produce a lubricated interface. Microscopically this behavior is produced by the orientation and stratification of collagen fibers and proteoglycans inside of the tissue (Jurvelin et al. 2000). All of the cartilage is porous and heavily hydrated but the superficial layer is predominantly type II collagen fibers oriented tangentially to the surface while the inner zones are less ordered and contain less collagen. The deeper layers contain significant amounts hydrophilic proteoglycans which bind water and encourage reabsorption of water after the tissue has been compressed. The overall structure of the cartilage is not unlike a cloth covered sponge bonded to the bone. As it is compressed water is exuded through the durable outside and it can only fully return to its original state by regaining the lost fluid to its softer inside.

## CHAPTER 2

### LITERATURE REVIEW

The importance of the health of biological soft tissues has been well established for many years. The direct relationship of articular cartilage degradation to the extremely painful condition of osteoarthritis (OA), the correlation between anterior cruciate ligament (ACL) injuries and OA, and the relatively recent connection of meniscus injury to initial OA symptoms have demonstrated that modeling these tissues is crucial to developing accurate limb level kinetic models (Fithian et al. 1990; Pozzi et al. 2010). Computational models are necessary to improve the overall understanding of the knee by providing approximations of values that cannot be directly measured and giving insight to the relationships of internal joint structures.

Previous modeling efforts have shown that it is important when constructing a knee model to represent the meniscus and it has been indicated that meniscus models should include representations of the anatomic constraints and the material nonlinearities and anisotropies. Typically the anisotropy of the meniscus is simplified to a cylindrical transversely isotropic representation with the circumferential stiffness being the dominate term.

Knee models that benefit from including a meniscus fall into two major categories, finite element (FE), and rigid body models. FE models are governed by detailed geometries and constitutive relationships which can be solved to produce accurate reproductions of tissue and single organ behavior. Adding the interactions of multiple bodies makes FE models become dramatically more complicated and increases the likelihood of encountering large displacements or deformations which FE models have difficulty handling. Rigid body models are governed by constraints on bodies and if surface geometry interaction is relevant its effect is applied through simplified interpenetration penalty functions. These models can easily and efficiently calculate

the behavior of multiple bodies that only undergo small deformations, but they are unable to determine behavior inside of a tissue.

Due to the known limitations of rigid body models few rigid multibody (MB) models have been created that incorporate a meniscus, the notable exception related to this work being the Guess et al. 2010 model which is the basis for much of the work described here (Guess et al. 2010). The Guess et al. 2010 model was created in MD.ADAMS 2010 and consisted of a rigid subject specific multibody skeleton (femur, patella, and tibia) and included deformable contacts, a flexible meniscus, and the major ligaments of the knee. This model was kinetically driven and validated kinematically against experimentally reproduced walk cycle data from the cadaver the model was based on. The addition of the meniscus to the model marginally improved kinematics and dramatically (32.6%) reduced the maximum contact force in the compartment with a healthy meniscus. FE knee models that include a meniscus are a little more common due to the methods capability of capturing deformable tissue behavior. Two examples of this are the models developed in Donahue et al. 2002 and Yao et al. 2006 both of these subject specific models were able to determine articular cartilage contact pressures and stresses while including the meniscus when subjecting their simulated knees to compression at fixed angles (Donahue et al. 2002; Yao et al. 2006). The Donahue et al. 2002 model studied the importance of boundary conditions to the knee level model while the Yao et al. 2006 model used design of experiments (DOE) to study the effects of meniscus parameters on the deformation error of the meniscus.

The meniscus models used by Donahue et al. 2002 and Yao et al. 2006 are very similar. Both models treated the meniscus as a transversely isotropic linearly elastic material with similar element size. The Yao et al. 2006 model possessed a much more sophisticated method for constraining the meniscus as many of the deformation parameters that were studied were

dependent on the menisci's attachments. The Yao et al. 2006 results indicated that the meniscus deformation was most dependent on the ratio of the transverse to circumferential modulus, the modulus of the peripheral attachments and the initial strain in the horn attachments.

Implementation of meniscus models in rigid multibody dynamic models is difficult but multibody tissue models have been developed and shown to perform adequately (Guess et al. 2010). This MB implementation consisted of a segmented meniscus model that was inserted into a larger previously developed knee model exhibiting multiscale modeling techniques that can be further expanded (Tawhai et al. 2009). The previous model was created using human data and the parameters defining the effective material properties of the menisci were determined from comparison to a linear FE model. The model developed in the current work is based off of canine data and the material properties have been determined experimentally. The experiment to tune the model consisted of a unique usage of a uniaxial tester to determine whole meniscus deformation behavior.

Articular cartilage of the knee/stifle is another biological soft tissue whose behavior can be difficult for rigid MB models. The comparatively soft and deformable nature of the articular surface can be approximated using geometry based interpenetration penalty functions. Unfortunately the penalty function parameters cannot be directly matched to material properties, and a tuning procedure must be used to obtain reasonable values. Experimental data was collected for this process using methods adapted from Shepherd & Seedhom 1997 and Jurvelin et al. 2000 (Shepherd and Seedhom 1997; Jurvelin et al. 2000). Both experiments involve the small scale indentation of articular cartilage in an attempt to determine material properties. The Shepherd & Seedhom data was collected off of human cadavers and was performed with a 1.5875mm radius spherical indenter. The Jurvelin data was collected on beagles (averaging 11.2 kg) and was done in a microindentation apparatus with a plane ended 0.4mm indenter. Both

models are modifications of contact theory to account for a soft material on a rigid substrate, the Shepherd & Seedhom model is empirically based and the Hayes et al. 1972 is physics based. A limited attempt to determine the material properties of the cartilage indentation samples collected for this work was performed after examining the modeling methods used in Shepherd and Seedhom 1997 and Hayes et al. 1972. The data collected here was unique in that it was canine based and performed on nearly intact articular surfaces

Accurate modeling of biological structures to determine the structural behavior and environment of joint tissues is vital to the development of truly helpful knee medicine. It has been demonstrated that components an individual's joint are composed of extremely specific geometry and material properties and that slight mismatches can produce radically unacceptable result. This has been demonstrated in a canine study where meniscal allograft replacement operations produced end outcomes for joint health that were as severe as total menisectomies (Elliott et al. 2002). With reliable modeling techniques to provide improved understanding of a patient's particular joint environment a healthier treatment may be determined.



## CHAPTER 3

### METHODS

#### **3.1 Experimental Testing**

For this work an experiment was created for the tuning of rigid MB models. This was an improvement over previous studies that relied on FE models that were known to exhibit some behavioral inaccuracies. For the testing of the menisci a novel whole meniscus test was developed where the tissue experienced a semi-physiological loading, consisting of a principally circumferential tension and compressive loadings in other orientations. For the cartilage the testing consisted of spherical indentation with an impervious indenter of 1 or 2 mm radius.

##### **3.1.1 Sample Preparation**

Canine stifle samples were provided by the Comparative Orthopedics Laboratory at the University of Missouri-Columbia. These samples were from the contralateral legs of 23-25 kg mongrel canines used in their research and were considered normal. Samples consisted of the distal 2-3" of the femur, the menisci, the proximal 3" of the tibia which had been sagittally bisected along the intercondylar notch (Figure 1). The stifles were fully disarticulated and wrapped in saline soaked gauze prior to freezing for shipping and storage.



Figure 1. A disarticulated canine stifle. Femur and tibia halves (left) and menisci (right)

### 3.1.2 Experimental Meniscus Testing

**Design of the testing fixture.** As the goal was to capture the behavior of the entire meniscus to produce one set of macroscopic parameters, an experiment was designed with the objective of loading a whole meniscus in a manner similar to its natural environment. As previously mentioned, in vivo the collagen fibers that make up the major structural component of the tissue are arranged circumferentially and are loaded in tension. Simulating this loading was the goal of the experimental portion of this study. To accomplish this each meniscus was stretched over a v-block that roughly conformed to the interior side (e.g. the medial side of the lateral meniscus) of the meniscus. This maintained the desired tension along the circumferential direction, and produced some compression in the radial and axial directions. The fixtures to hold the sample in the uniaxial tester and the v-block were designed in SolidWorks (Dassault Systemes Solidworks Corp., Concord, Ma). The V-block was a 6 or 12mm wide block with a "V" shaped channel removed from one surface (Figure 2). The v-block's channel was created

from a lofted shape comprised of a series of three triangles which was then cut from the surface along an elliptical path. The path and dimensions of the triangles were visually estimated from the comparison of 3 meniscus geometries so that the three triangles approximately corresponded to the anterior, central, and posterior portions of the menisci. Due to receiving an incomplete MRI the lateral v-blocks channel was only created from 2 geometries at the central portion. The final V-blocks were composed of ABSplus and were produced in a Dimension bst1200es 3D printer with a layer resolution of 0.1".

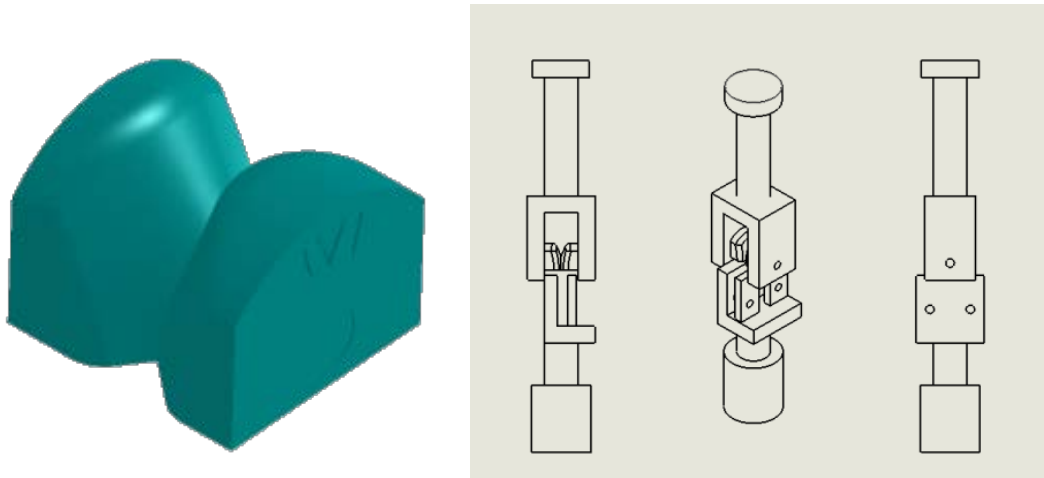


Figure 2. A 3D model of the lateral meniscus v-block

6 mm and 12 mm width versions of the medial and lateral v-blocks were produced to provide a variable boundary condition. The goal of this was to produce two separate but related datasets that could be used to create a robust set of meniscus parameters that would be insensitive to the specific loading behavior.

**Experimental procedure.** A Bose ELF-3300 electromechanical uniaxial tester was used to implement this procedure and the data was collected with the Wintest (Bose, Eden Prairie, MN) software. After being aligned in the v-block the menisci were clamped near the

horn attachments by metal vise plates lined with sandpaper and tightened by thumbscrews (Figure 3). The samples were then subjected to two different loading scenarios: a 0.2Hz sinusoidal load for 20s and a 5s ramp. The loading values varied from trial to trial based on our confidence in the ability of the vises to hold without slipping. For the data used here load profiles consisting of 8N/s (0.1N preload) ramps and sinusoidal (0.2Hz 4N to 50N) waves were applied. The third canine meniscus sample (stifle 2R) was tested on a Bose ELF-3200 due to a broken load cell rendering the ELF-3300 out of order. During the course of the testing the tissue samples were regularly sprayed with a PBS solution.

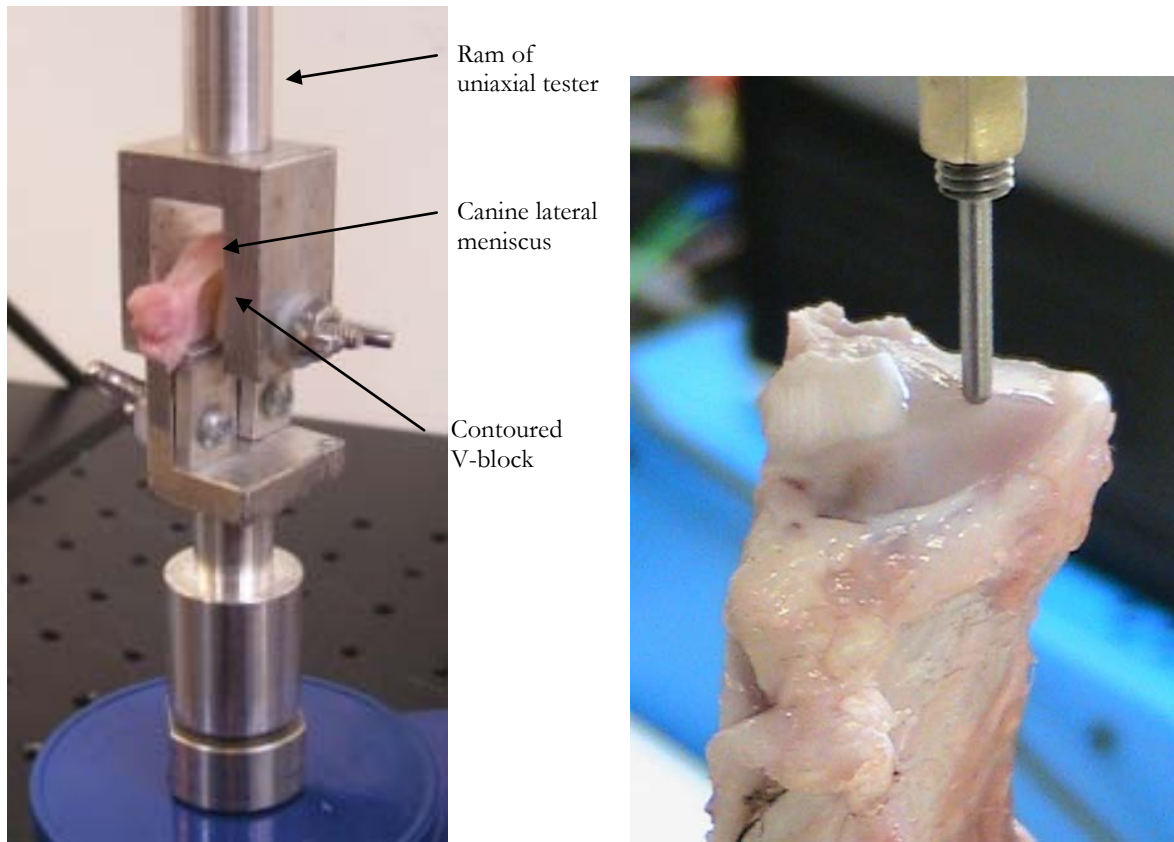


Figure 3. Meniscus testing apparatus (left) and cartilage indentation (right).

The ELF machine recorded the commanded profiles as well as the vertical position and force in the ram at a sample rate of 100Hz. Stifle 14L was tested on October 1, 2009; stifle 11L, on July 22 2009; stifle 2R, on April 9, 2010.

### 3.1.3 Experimental Cartilage Testing

The tibia halves were potted in ABSplus semi-cylindrical cups using auto body filler (Bondo, 3M, St. Paul, MN) prior to being inserted into the testing platform. This set up allowed complete axial rotation of the sample, and limited motion and rotation in 3 other degrees of freedom (Figure 4). The objective of this test platform was to allow the positioning of the sample to achieve an indentation result that was normally oriented to the intact articular surface (Figure 3). The indentation was performed in force control with the commanded force rising over 5s to a load of 9.45N for the 2mm indenter and to a load of 2.36N for the 1mm indenter.

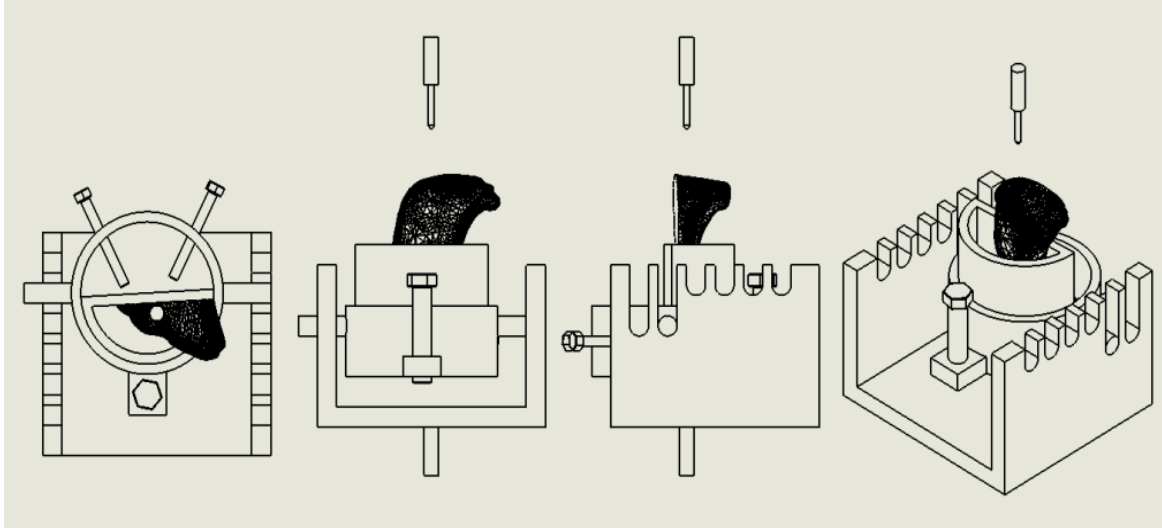


Figure 4. A schematic sketch of the indentation apparatus (with tibia half)

This ELF machine also recorded the commanded profiles as well as the vertical position and force in the ram at a sample rate of 100Hz.

## 3.2 Model Creation

The model creation process entailed herein is an adaptation of the process described in Guess et al. 2010.

### 3.2.1 Geometry Creation

**Rough geometry generation.** MRI's of the intact canine stifles were taken in the sagittal and coronal planes prior to disarticulation. The MRI's were then used in conjunction with the 3D Slicer (www.Slicer.org) software package to generate 3D geometry models of the canine menisci. This is done by manually segmenting each image slice of the sagittal MRI into the desired tissues, in this case the femur, patella, tibia, tibial cartilage, sesamoids and the meniscus (Figure 5). The accuracy of this process is limited by the MRI resolution (field strength 1.5T, TE 86, TR 44, 2.2 mm slice spacing,, pixel resolution of 0.391 x 0.391 resolution), the machine operator's ability to produce a clear image with distinguishable differences in tissues, and the interpretation of the MRI. This method can produce very accurate geometries but unfortunately the MRI's resolution was mediocre for this type of work, particularly in the direction of slicing. Once the segmentation of the tissues was complete 3D Slicer was used to generate coarse STL geometries of the tissues (Figure 6).

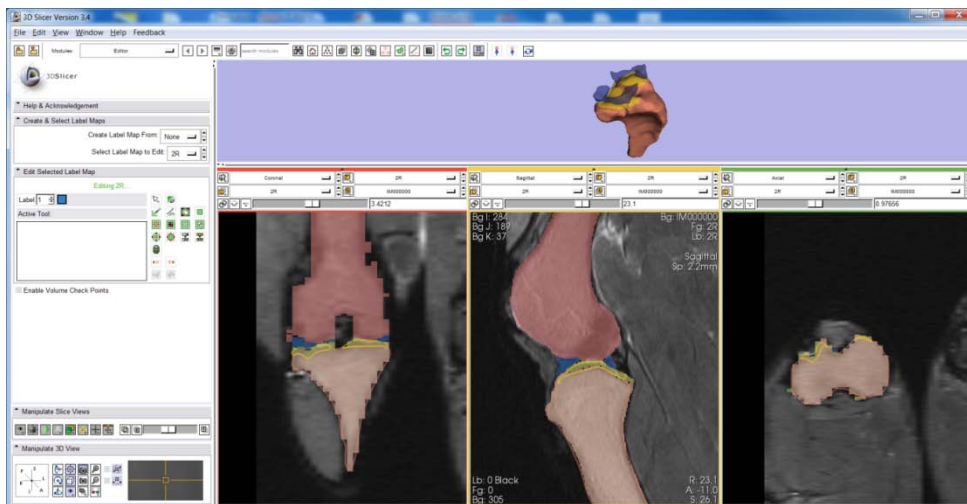


Figure 5. 3D Slicer sample window, showing a sagittal MRI with traces in all three planes

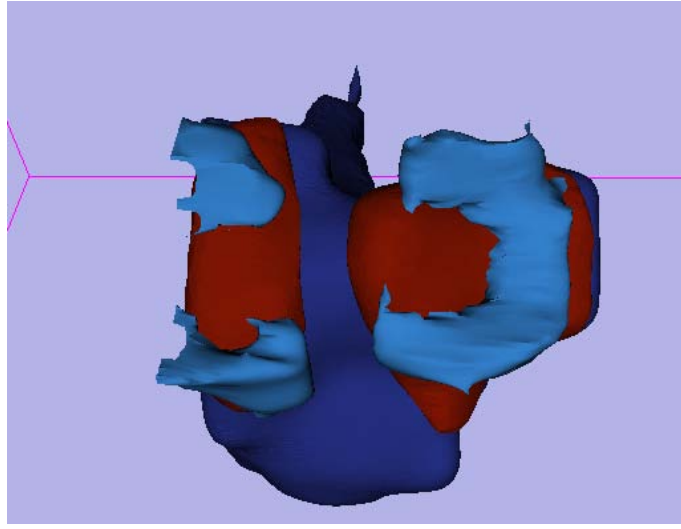


Figure 6. Course geometry for a canine tibia, cartilage and meniscus (incomplete)

**Smoothed geometry generation.** 3D Slicer does have some capability to smooth the models as it produces them but this was utilized only slightly as geometry smoothing can be performed with much more control in Geomagic Studio 11 (Geomagic, inc. Research Triangle Park, NC ). The slight smoothing that was performed in Slicer was to take advantage of its internal routine to ensure the final geometries did not intersect. In Geomagic, extensive use of the offset, reduce noise, clean, mesh doctor, hole fill, and decimate tools produced final geometries that were not excessively complex but still smooth in appearance (Figure 7). The accuracy of the models after post processing were qualitatively confirmed by importing them to 3D Slicer and using the model intersection functionality. This function calculates the outline of a geometry's intersection with the MRI's slice planes (Figure 8). In some cases photo overlays were used to confirm meniscus geometries (Figure 9).

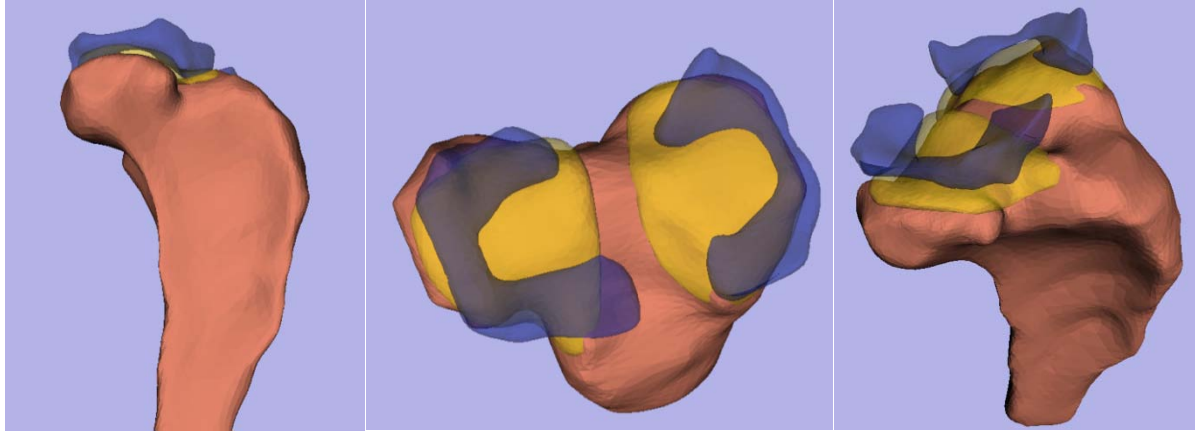


Figure 7. Smoothed geometries after post processing in Geomagic Studio.



Figure 8. Post processed geometries intersected onto the MRIs for verification



Figure 9. A photo overlay of the smoothed geometries (meniscus in blue, cartilage in yellow, and tibia in red) and the original sample.



### 3.2.2 Elastic Behavior Modeling

**Transverse isotropic elastic implementation for meniscus.** After the meniscus geometry is generated and radially segmented each segment is connected to its neighbor via an ADAMS field element. The center of rotation for both the segmentation and the field element orientation is located 2 mm to the center of the knee from where the meniscus rests in vivo. An ADAMS field element is a combination 6-axis spring damper, where the force displacement relationship is defined as (MD ADAMS 2010 help.):

$$\begin{bmatrix} F_x \\ F_y \\ F_z \\ T_x \\ T_y \\ T_z \end{bmatrix} = - \begin{bmatrix} K_{11} & K_{12} & K_{13} & K_{14} & K_{15} & K_{16} \\ K_{21} & K_{22} & K_{23} & K_{24} & K_{25} & K_{26} \\ K_{31} & K_{32} & K_{33} & K_{34} & K_{35} & K_{36} \\ K_{41} & K_{42} & K_{43} & K_{44} & K_{45} & K_{46} \\ K_{51} & K_{52} & K_{53} & K_{54} & K_{55} & K_{56} \\ K_{61} & K_{62} & K_{63} & K_{64} & K_{65} & K_{66} \end{bmatrix} \begin{bmatrix} x - x_0 \\ y - y_0 \\ z - z_0 \\ a - a_0 \\ b - b_0 \\ c - c_0 \end{bmatrix} - \begin{bmatrix} C_{11} & C_{12} & C_{13} & C_{14} & C_{15} & C_{16} \\ C_{21} & C_{22} & C_{23} & C_{24} & C_{25} & C_{26} \\ C_{31} & C_{32} & C_{33} & C_{34} & C_{35} & C_{36} \\ C_{41} & C_{42} & C_{43} & C_{44} & C_{45} & C_{46} \\ C_{51} & C_{52} & C_{53} & C_{54} & C_{55} & C_{56} \\ C_{61} & C_{62} & C_{63} & C_{64} & C_{65} & C_{66} \end{bmatrix} \begin{bmatrix} V_x \\ V_y \\ V_z \\ \omega_x \\ \omega_y \\ \omega_z \end{bmatrix} + \begin{bmatrix} F_1 \\ F_2 \\ F_3 \\ T_1 \\ T_2 \\ T_3 \end{bmatrix} \quad \text{Eq. 1}$$

where  $F_b$ ,  $T_b$ ,  $K$ , and  $C$  are forces, torques, stiffness matrix, and damping matrix respectively and  $x, y, z$  are locations and  $a, b, c$  are orientations. By stipulating that menisci exhibit a transverse isotropic behavior the  $K$  matrix can be simplified to:

$$\begin{bmatrix} K_\theta & K_{\theta r} & K_{\theta z} & 0 & 0 & 0 \\ K_{\theta r} & K_r & K_{rz} & 0 & 0 & 0 \\ K_{\theta z} & K_{rz} & K_z & 0 & 0 & 0 \\ 0 & 0 & 0 & T_\theta & 0 & 0 \\ 0 & 0 & 0 & 0 & T_r & 0 \\ 0 & 0 & 0 & 0 & 0 & T_z \end{bmatrix} \quad \text{Eq. 2}$$

Also for the purpose of simplicity the  $C$  matrix was calculated as a coefficient  $C$  multiplied by the  $K$  matrix. The field elements were aligned so that the  $\theta$  direction was circumferentially aligned, the  $r$  direction was radially aligned, and the  $z$  direction was along the superior/inferior axis.

**Nonlinear implementation.** The principle load bearing component of menisci is collagen. It has been shown that ligaments, another collagen heavy soft tissue, exhibit a reproducible and consistent nonlinearity. This nonlinearity is explained by the presence of crimped collagen fibers that have to undergo some strain prior to being recruited to bear any significant load. Mathematically this has been represented repeatedly by a series of piecewise equations. To represent this initial strain hardening the stiffness in tension is calculated as a parabola leading to a continuous straight line at a fixed strain. For a ligament, which buckles under any compressive load, the mathematical representation produces zero force in compression. In this work the  $K_0$  component has been reformulated into a similar piecewise equation.

$$f = \begin{cases} \frac{1}{4}kx^2/x_l & 0 \leq x \leq 2x_l \\ k(x - x_l) & 2x_l < x \\ -\frac{1}{4}kx^2/x_l & 0 > \geq 2x_l \\ -k(x - x_l) & -2x_l > x \end{cases} \quad \text{Eq.3}$$

Where  $k$  is a stiffness value,  $x$  is the  $\theta$  displacement, and  $x_l$  is half the length of the nonlinearity. The principle differences between this formulation and that described for ligament behavior is that it is displacement not strain based and that the compression curve is a reflection of the tension curve rather than a 0 value. A user defined library with the modified field element formulation was written in C++ and compiled for use in the ADAMS software.

**Contact function.** The second method of modeling deformable materials that is available in ADAMS consists of a penalty function describing interpenetration of geometries. This contact formulation is by default defined as:

$$F = k\delta^{exp} + B(\delta)\dot{\delta} \quad \text{Eq.4}$$

Where  $F$  is the force produced,  $k$  is a contact stiffness,  $exp$  is an exponent greater than 1,  $B$  is a damping value and  $\delta$  and  $\dot{\delta}$  are the interpenetration depth and velocity. For the thin layer

of cartilage this is the only mechanism available for reproducing its behavior and must be tuned to experimental data. For the meniscus it was decided to leave the contact values at an arbitrary constant value shown in Table 1. These values were chosen for two separate reasons. The chosen values are stiff enough that whole meniscus flexion and translation dominate its behavior in compression; this was seen as a reasonable assumption due to the high water content of the meniscus which should limit transient and excessive localized deformation. These conditions also simulated well as they produced low computation time and created a model with an insignificant chance of a geometry passing through the meniscus geometry.

Table 1. Contact parameters used for meniscus on v-block interaction

| <b>Parameter</b>       | <b>Value</b> |
|------------------------|--------------|
| Stiffness (N/mm)       | 5000         |
| Damping (N·s/m)        | 2.5          |
| Force Exponent         | 2.25         |
| Penetration Delta (mm) | 0.001        |

### 3.2.3 ADAMS Model Creation

**Meniscus segmentation.** After the creation of the final meniscus geometries in Geomagic Studio the STL files were converted to IGES files and imported into ADAMS and oriented with the global coordinate. Segmentation was performed via an ADAMS command language macro that duplicated the geometry of a meniscus and then intersected it with a cylinder segment. In this study the center of rotation about which the wedges were produced was 2mm away from the calculated center of mass of the meniscus. Another macro was used to generate and align the field elements between the segments.

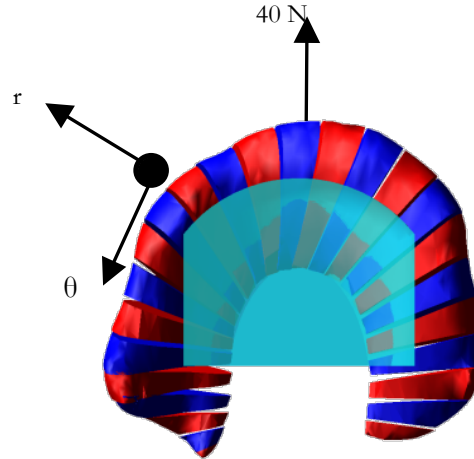


Figure 10. Multibody meniscus under load.

### 3.3 Model Execution.

**Meniscus model Setup/Alignment.** After the meniscus had been segmented and the field elements were created they were moved as a group and aligned to a virtual reproduction of the experimental apparatus (Figure 10). Alignment was done initially based on photos taken along the anterior/posterior axis of the meniscus. The known geometries of the experimental apparatus were used to determine scaling coefficients and measurements to points on the experimental apparatus were used to determine rough position. This allowed for reasonable alignment but did not resolve rotations about the v-block. Additional alignment was then done by simulating springs attached to the horns of the meniscus. The meniscus was then moved down (less than 1 mm in .1 mm increments) far enough to ensure contact was made with the v-block. A sufficient amount of contact was deemed to have been achieved when a transient peak of at least 1N was produced in the springs that diminished to at least a 0.05 N at steady state. During this transient period (1 second was allowed) the multibody meniscus was allowed to conform to the v-block, the material parameters during this conformation were those listed as the initial parameter values in Tables 4, 5, 6, and 7. These springs were then removed and

replaced with a spherical joint with a 0.3 coefficient of static friction and a 0.1 coefficient of dynamic friction. This new position was assumed to be close to the starting position of the meniscus after it had been inserted into the v-block and the horns had been held by the vises. The variables that were examined in this experiment were the 9 distinct values in the  $K$  matrix, the damping ratio,  $DR$ , the nonlinear length variable,  $x_i$ , and the initial displacement correction,  $iDisp$ . The blind estimate of properties for these variables were estimated as the average of the lateral and medial meniscus values from Guess et al. 2010 and the  $K_\theta$  value was increased by 20% to account for the softening effect of modeling the nonlinear behavior.

**Model execution.** In the ADAMS model a vertical force was applied to the upper fixture/v-block assembly and the displacement was compared to the measured displacement. The first second of simulation time applied a variable displacement correction to the initial position of the meniscus. This variable was to account for the unmeasured initial strain in the meniscus that was produced while placing the meniscus into the experimental apparatus. The variable was optimized based on the logic that the error would be minimal when the distraction produced by this displacement most nearly matched that of the experiment. The recorded data profiles from the experimental portion included time periods before and after the experimental loading profile. Prior to importing the load and displacement profiles into ADAMS as splines some limited preprocessing is performed. This preprocessing consisted of filtering the data in Matlab at 10Hz using a forwards and backwards 2<sup>nd</sup> order low-pass Butterworth filter and trimming the data. The trimming process removes 20s of data starting at the point the deformation velocity reached 50 mm/s as determined by the Matlab gradient algorithm, a modified central difference method. This criterion was used to determine the starting point of the loading profile as a means to remove an anomalous transient behavior that was consistently

observed at the beginning of each trial. The meniscus models were run in ADAMS with a step size of 0.02Hz.

It was rapidly noticed that the thinnest portion of the meniscus closest to the intercondylar notch produced unusual contact behavior against the v-block. To mitigate this behavior the nadir of the v-block was eliminated by removing a 1mm thick slice from the v-block.

**Cartilage Model.** This work is currently ongoing but presently the cartilage models consist of two stacked flat cylinders, the lower represents the bone and is 1mm tall; the upper is the thickness of the cartilage and represents the cartilage. For the cartilage models it is assumed that the effects of curvature are not significant. A cartilage thickness was estimated from the MRI's and overhead photos of the indentation site. An ADAMS macro is being used to segment the cartilage block into 0.5 mm square pieces, fix their position to the bone cylinder, and create contact parameters between the cartilage segments and a model of the indenter. The primary objective of this model is to establish baseline values for the contact parameters when modeling cartilage. To this end some elastic moduli were calculated to ascertain the validity of the experimental data. The moduli selected for this procedure were simple Hertzian contact of a sphere on an infinite half-space (Eq. 5), the Waters formulation correcting for a soft material of finite depth on a rigid surface (Eq. 6), and the Hayes formulation correcting for the same effect (Eq. 7).

$$E = \frac{3P(1-\nu)(1+\nu)}{8\sqrt{R}\delta^{3/2}} \quad \text{Eq. 5}$$

$$E_2 = \frac{9P}{16\sqrt{R}} \left( \frac{1 - e^{-0.42h/\sqrt{2R\delta - \delta^2}}}{\delta} \right) \quad \text{Eq. 6}$$

$$E_3 = \frac{P(1-\nu)^2}{2a\kappa\delta} \quad \text{where } \chi = \frac{a^2}{\delta R} \quad \text{Eq. 7}$$

For these equations  $P$  is load,  $\delta$  is penetration depth,  $R$  is indenter radius, and  $\nu$  is Poisson's ratio equal to 0.5 (Shepherd and Seedhom 1997). For the Hayes equation  $a$  is the radius of the contact patch and  $\chi$  and  $b$  are used in a lookup table to determine the correct  $a$  and  $\kappa$  values in an iterative process (Hayes et al. 1972).

### 3.4 Design of Experiments.

ADAMS/Insight was used for statistical calculation and optimization in the design of experiments portion of the study. Initial values for the 9 stiffness and the damping ratio values were estimated and screened using a 32 run resolution IV 2-level fractional factorial design. These initial values came from the Guess 2010 parameters for human meniscus and experimentation with the incomplete lateral 11L geometry. These still rough values were then optimized using a 155 run central composite design, minimizing the objective of the RMS. Another resolution IV design was performed to screen the variables down to 4 significant terms ( $p < .05$ ) and the damping ratio which were again optimized using a central composite design (CCD). Additional CCD's were performed until the objective function produced less than a 5% reduction in error. All optimization was performed on sinusoidal datasets which were expected to be more physiological. As verification errors for ramp trials were calculated with the models using the optimum values as determined for the corresponding sinusoidal trials.

Unfortunately, for some of the models a memory build up error prevented the successful completion of a 155 run CCD. In these instances multiple 5 and 6 level CCD's were performed with various combinations of the 12 variables.

## CHAPTER 4

### RESULTS

#### **4.1 Experimental Testing**

##### **4.1.1 Experimental Meniscus Testing**

As was earlier stated the loading values varied from trial to trial based on our confidence in the ability of the vises to hold without slipping. Additionally, some of the experiments were performed on the Bose ELF 3300 and some on the ELF 3200, while these should have had near identical performance in this load-displacement range some discrepancy was observed. This was probably caused by the PID control mechanism being tuned for the smaller loads seen in the cartilage testing. The ramp trials from the ELF 3200 were only simulated until 95.02% of the max load as this corresponds to 3 time constants of decay in what appeared to be an exponentially decaying error; this keeps the simulations to similar time lengths. The loading values for the various trials and samples are displayed in table 2. As the trials were performed in force control the command profile shown in figures 14, 15, 16, and 17 should be proportional to the desired force.



Table 2. List of valid meniscus test data.

| Knee  | File Name         | Side    | V-block Width | Loading Pattern | Load Max (approx) | Modeled |
|-------|-------------------|---------|---------------|-----------------|-------------------|---------|
| 11L   | 11LMedNarrow1     | Medial  | N             | Ramp            | 40                |         |
| 11L   | 11LMedNarrow2     | Medial  | N             | Ramp            | 60                |         |
| 11L   | 11LMed1           | Medial  | W             | Ramp            | 38                |         |
| 11L   | 11LMed2           | Medial  | W             | Ramp            | 58                | X       |
| 11L   | 11LMedsine102     | Medial  | W             | Sine            | 60                | X       |
| 14L   | 14Llateralw       | Lateral | W             | Ramp            | 40                |         |
| 14L   | 14Llateralw3      | Lateral | W             | Ramp            | 58                |         |
| 14L   | 14Llateraln2      | Lateral | N             | Ramp            | 40                | X       |
| 14L   | 14Llateraln3      | Lateral | N             | Ramp            | 60                |         |
| 14L   | 14Llateraln4      | Lateral | N             | Ramp            | 80                |         |
| 14L   | 14Llateralnsine02 | Lateral | N             | Sine            | 50                | X       |
| 14L   | 14Llateralnsine2  | Lateral | N             | Sine            | 50                |         |
| 14L   | 14Lmedial         | Medial  | W             | Ramp            | 27                |         |
| 14L   | 14Lmedial2        | Medial  | W             | Ramp            | 22                |         |
| Blank | Rubbertest        | Blank   | W             | Ramp*           | 20                |         |
| 2R    | 2RmedWdf          | Medial  | W             | Ramp*           | 12                |         |
| 2R    | 2RmedNdf          | Medial  | N             | Ramp*           | 20                |         |
| 2R    | 2RmedN2df         | Medial  | N             | Ramp*           | 45                |         |
| 2R    | 2RmedNsine        | Medial  | N             | Sine*           | 26                |         |
| 2R    | 2RLatN            | Lateral | N             | Ramp*           | 40                | X       |
| 2R    | 2RLatNsine        | Lateral | N             | Sine*           | 28                | X       |
| 2R    | 2RlatW            | Lateral | W             | Ramp*           | 65                |         |
| 2R    | 2RLatWsine        | Lateral | W             | Sine*           | 38                | X       |
| 2R    | 2rLatW2           | Lateral | W             | Ramp*           | 99                | X       |
| 2R    | 2RlatW3           | Lateral | W             | Ramp*           | 145               |         |

\*Pertains to data collected on the ELF-3200

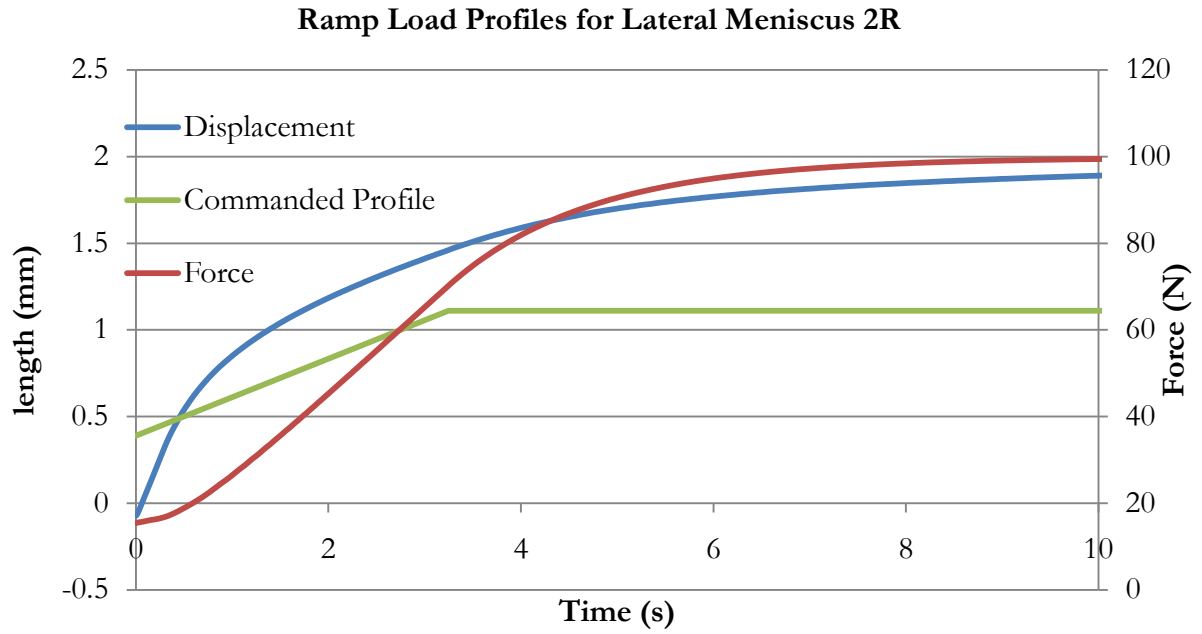


Figure 11. A representative ramp loading profile for 2R

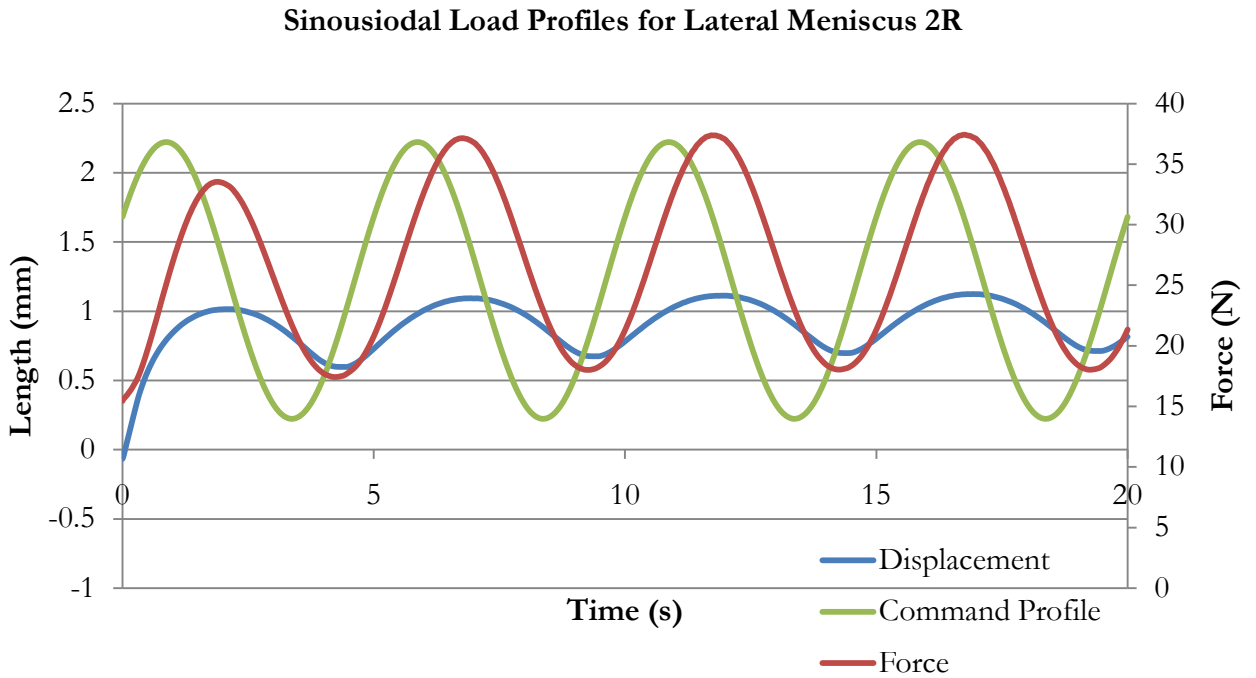


Figure 12. A representative sine loading profile for 2R

### Ramp Load Profiles for Medial Meniscus 11L

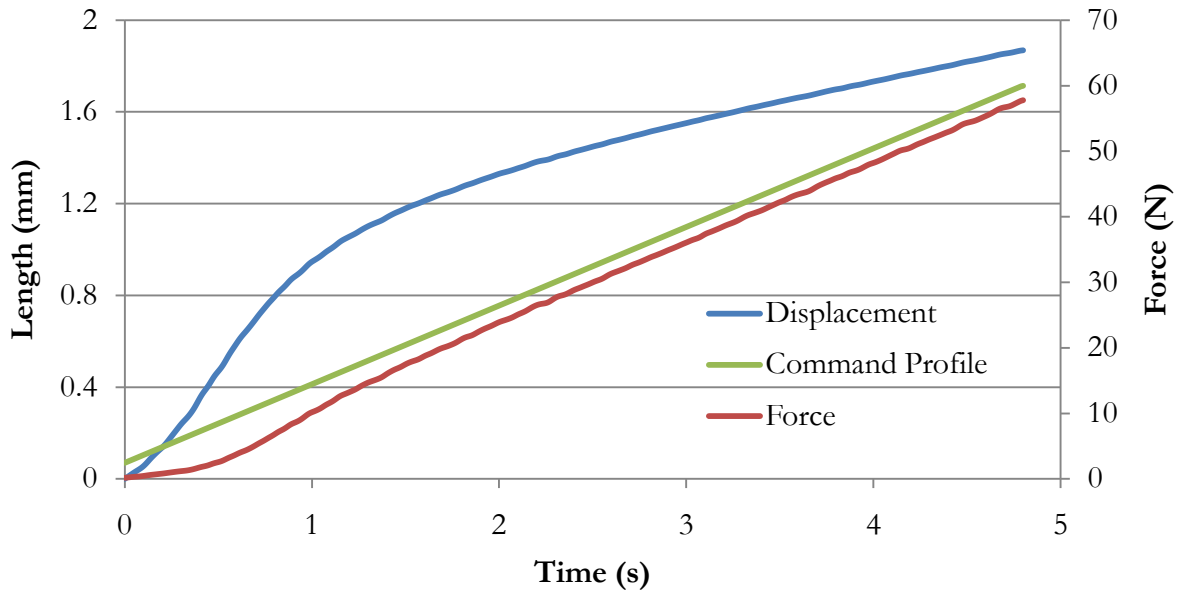


Figure 13. A representative ramp loading profile for 11L

### Sinusoidal Load Profiles for Medial Meniscus 11L

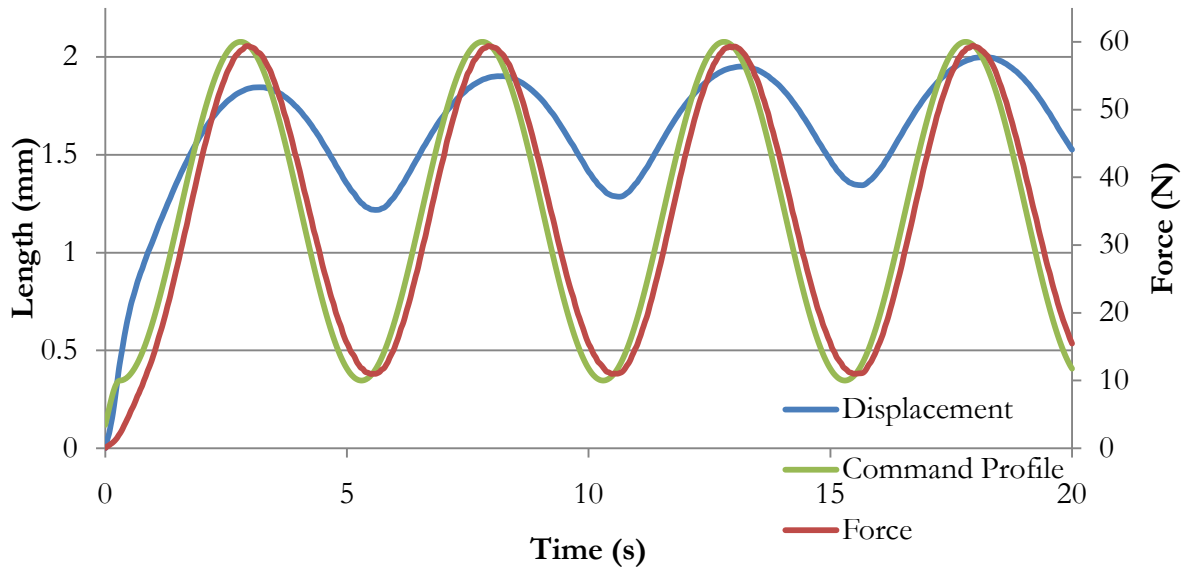


Figure 14. A representative sine loading profile for 11L

#### 4.1.2 Experimental Cartilage Testing

The tibia sample holder was designed with the objective of allowing for perpendicular indentation points to be taken. This was observed to have been achieved with a high degree of success for 2 out of the 3 samples taken per tibia halve. The loading values for the indentation trials in this study are shown in table 3.

Table 3. Indentation samples

| Knee | Side    | Indenter Radius (mm) | Loading Pattern |
|------|---------|----------------------|-----------------|
| 11L  | Medial  | 2                    | Ramp            |
| 11L  | Medial  | 1                    | Ramp            |
| 11L  | Lateral | 2                    | Ramp            |
| 11L  | Lateral | 1                    | Ramp            |

| Knee | Side    | Indenter Radius (mm) | Loading Pattern |
|------|---------|----------------------|-----------------|
| 14L  | Medial  | 2                    | Ramp            |
| 14L  | Medial  | 2                    | Ramp            |
| 14L  | Medial  | 1                    | Ramp            |
| 14L  | Lateral | 1                    | Ramp            |
| 14L  | Lateral | 1                    | Ramp            |
| 14L  | Lateral | 2                    | Ramp            |

| Knee | Side    | Indenter Radius (mm) | Loading Pattern |
|------|---------|----------------------|-----------------|
| 2R   | Medial  | 2                    | Ramp            |
| 2R   | Medial  | 1                    | Ramp            |
| 2R   | Medial  | 1                    | Ramp            |
| 2R   | Lateral | 1                    | Ramp            |
| 2R   | Lateral | 2                    | Ramp            |
| 2R   | Lateral | 2                    | Ramp            |

## 4.2 Model Results

### 4.1.3 Elastic Behavior Modeling

The ADAMS field element with a nonlinear circumferential stiffness was successfully created. Figure 15 is a sample force-displacement graph with a stiffness of 5 N/mm (slope of the linear region) a nonlinear length parameter of 1mm (the toe region is 4 mm wide), and a damping ratio of 0.05 (determines hysteresis width).

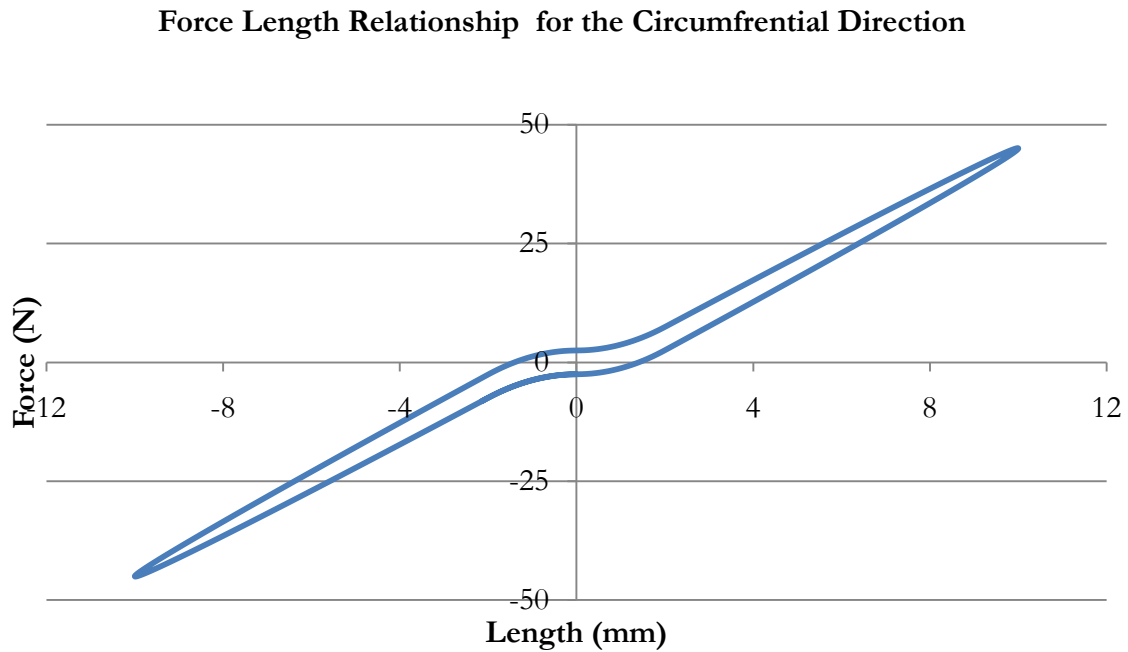


Figure 15. Graphical example of nonlinear force length behavior

### 4.2.1 Meniscus Results

The ADAMS results for the menisci provide the following errors when compared to the experimental data (Tables 4, 5, 6, 7, and 8).

Table 4. Optimized parameters and errors for the medial 11L meniscus.

| Wide                  |         |           |
|-----------------------|---------|-----------|
| Parameters            | Initial | Optimized |
| $K_\theta$ (N/mm)     | 408     | 1093      |
| $K_{\theta_r}$ (N/mm) | 52.5    | 1.83      |
| $K_{\theta_s}$ (N/mm) | 55      | 1.875     |
| $K_r$ (N/mm)          | 282     | 103       |
| $K_{r_s}$ (N/mm)      | 50.25   | 9.14      |
| $K_s$ (N/mm)          | 330     | 96.4      |
| $T_\theta$ (Nmm/deg)  | 46.25   | 2.58      |
| $T_r$ (Nmm/deg)       | 39.75   | 2.42      |
| $T_s$ (Nmm/deg)       | 46.75   | 50*       |
| DR                    | 0.4     | 0.225     |
| $X_l$ (mm/FIE )       | 0.01    | 0.0336    |
| $iDisp$               | -0.1    | 0.69      |
| Sine RMSE             | 0.777   | 0.107     |
| Ramp RMSE             | 0.772   | 0.067     |

Table 5. Optimized parameters and errors for the lateral 2R meniscus.

| Wide                  |         |           |
|-----------------------|---------|-----------|
| Parameters            | Initial | Optimized |
| $K_\theta$ (N/mm)     | 408     | 5780      |
| $K_{\theta_r}$ (N/mm) | 52.5    | 2.25      |
| $K_{\theta_s}$ (N/mm) | 55      | 2.5       |
| $K_r$ (N/mm)          | 282     | 98.4      |
| $K_{r_s}$ (N/mm)      | 50.25   | 7.5       |
| $K_s$ (N/mm)          | 330     | 123       |
| $T_\theta$ (Nmm/deg)  | 46.25   | 33.8      |
| $T_r$ (Nmm/deg)       | 39.75   | 9.17      |
| $T_s$ (Nmm/deg)       | 46.75   | 31.2      |
| DR                    | 0.4     | 0.330     |
| $X_l$ (mm/FIE )       | 0.01    | 0.00940   |
| $iDisp$               | -0.1    | -0.833    |
| Sine RMSE             | 0.647   | 0.0523    |
| Ramp RMSE             | 0.818   | 0.167     |

Table 6. Optimized parameters and errors for the lateral 2R meniscus.

| Narrow                |         |           |
|-----------------------|---------|-----------|
| Parameters            | Initial | Optimized |
| $K_\theta$ (N/mm)     | 408     | 600       |
| $K_{\theta_r}$ (N/mm) | 52.5    | 2.25      |
| $K_{\theta_x}$ (N/mm) | 55      | 2.5       |
| $K_r$ (N/mm)          | 282     | 55.6      |
| $K_{r_x}$ (N/mm)      | 50.25   | 3.75      |
| $K_x$ (N/mm)          | 330     | 167       |
| $T_\theta$ (Nmm/deg)  | 46.25   | 33.8      |
| $T_r$ (Nmm/deg)       | 39.75   | 18.7      |
| $T_x$ (Nmm/deg)       | 46.75   | 114       |
| $DR$                  | 0.4     | 0.225     |
| $X_f$ (mm/FIE )       | 0.01    | 0.00675   |
| $iDisp$               | -0.1    | 0.05      |
| Sine RMSE             | 0.199   | 0.0584    |
| Ramp RMSE             | 0.288   | 0.170     |

Table 7. Optimized parameters and errors for the lateral 14L meniscus.

| Narrow                |         |           |
|-----------------------|---------|-----------|
| Parameters            | Initial | Optimized |
| $K_\theta$ (N/mm)     | 408     | 307       |
| $K_{\theta_r}$ (N/mm) | 52.5    | 2.25      |
| $K_{\theta_x}$ (N/mm) | 55      | 2.5       |
| $K_r$ (N/mm)          | 282     | 156       |
| $K_{r_x}$ (N/mm)      | 50.25   | 7.5       |
| $K_x$ (N/mm)          | 330     | 92.6      |
| $T_\theta$ (Nmm/deg)  | 46.25   | 5.63      |
| $T_r$ (Nmm/deg)       | 39.75   | 4.67      |
| $T_x$ (Nmm/deg)       | 46.75   | 33.6      |
| $DR$                  | 0.4     | 0.211     |
| $X_f$ (mm/FIE )       | 0.01    | 0.0922    |
| $iDisp$               | -0.1    | 0.287     |
| Sine RMSE             | 1.75    | 0.328     |
| Ramp RMSE             | 0.409   | 0.910     |

Table 8. Summary of errors

| Error per Meniscus |      |          |                |        |
|--------------------|------|----------|----------------|--------|
|                    |      | RMS (mm) | Max Disp. (mm) | NRMS   |
| 11L Wide           | sine | 0.107    | 2.00           | 0.0535 |
|                    | ramp | 0.067    | 1.87           | 0.0359 |
| 2R Wide            | sine | 0.0523   | 1.12           | 0.0465 |
|                    | ramp | 0.167    | 1.77           | 0.0946 |
| 2R Narrow          | sine | 0.0584   | 1.01           | 0.0576 |
|                    | ramp | 0.170    | 1.06           | 0.161  |
| 14L Narrow         | sine | 0.328    | 3.46           | 0.0947 |
|                    | ramp | 0.910    | 2.08           | 0.438  |
| Average            |      | 0.232    | 1.80           | 0.123  |

Table 9. Collected parameters values for the MB canine meniscus.

| Nominal Values        |       |        |         |
|-----------------------|-------|--------|---------|
|                       | Mean  | Median | Average |
| $K_\theta$ (N/mm)     | 1945  | 847    | 1396    |
| $K_{\theta_r}$ (N/mm) | 2.15  | 2.25   | 2.20    |
| $K_{\theta_x}$ (N/mm) | 2.34  | 2.50   | 2.42    |
| $K_r$ (N/mm)          | 103   | 101    | 102     |
| $K_{r_x}$ (N/mm)      | 7.0   | 7.5    | 7.2     |
| $K_x$ (N/mm)          | 120   | 110    | 115     |
| $T_\theta$ (Nmm/deg)  | 19.0  | 19.7   | 19.3    |
| $T_r$ (Nmm/deg)       | 8.74  | 6.92   | 7.83    |
| $T_x$ (Nmm/deg)       | 59.6  | 33.6   | 46.6    |
| DR                    | 0.248 | 0.225  | 0.236   |

Table 10. RMS errors for models when using nominal parameter values

|              |      | Mean  | Median | Average |
|--------------|------|-------|--------|---------|
| 11L          | sine | 1.53  | 0.926  | 0.126   |
|              | ramp | 0.922 | 0.785  | 0.876   |
| 2R<br>Wide   | sine | 1.02  | 1.11   | 1.04    |
|              | ramp | 1.4   | 1.59   | 1.47    |
| 2R<br>Narrow | sine | 0.118 | 0.124  | 0.11    |
|              | ramp | 0.119 | 0.198  | 0.139   |
| 14L          | sine | 1.14  | 0.765  | 0.997   |
|              | ramp | 0.158 | 0.383  | 0.201   |
| Average      |      | 0.801 | 0.735  | 0.620   |



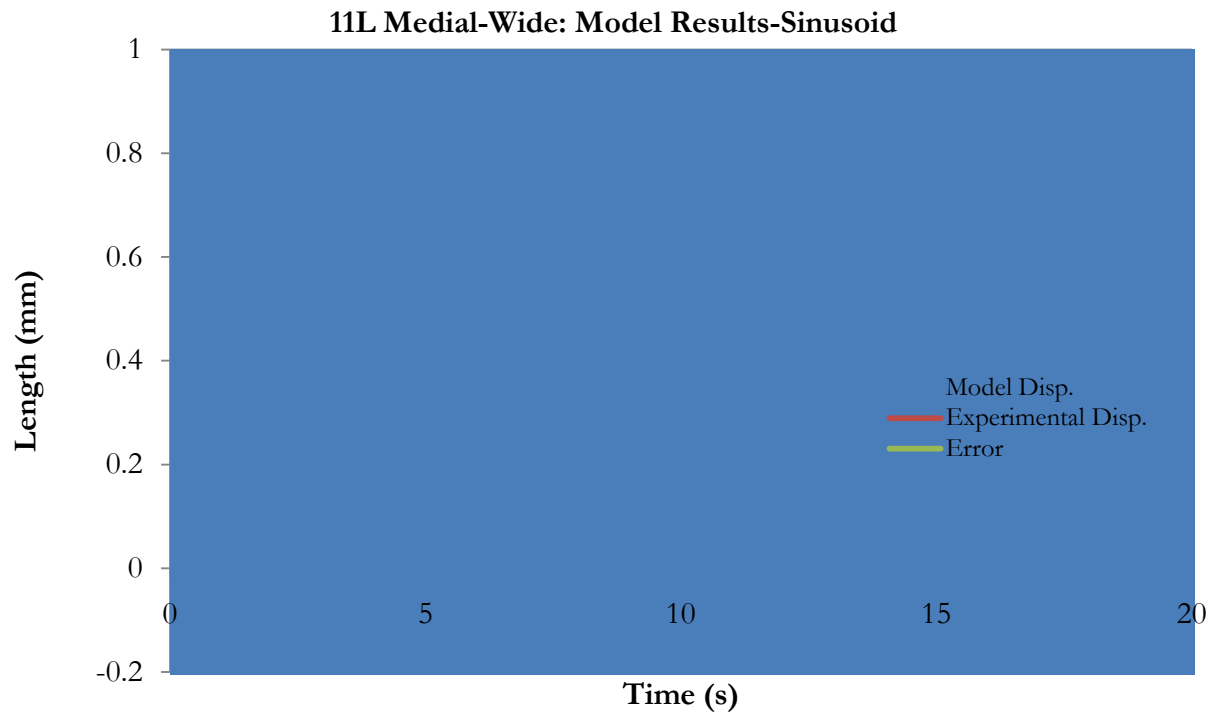


Figure 16. MB meniscus results for 11L Medial-Wide

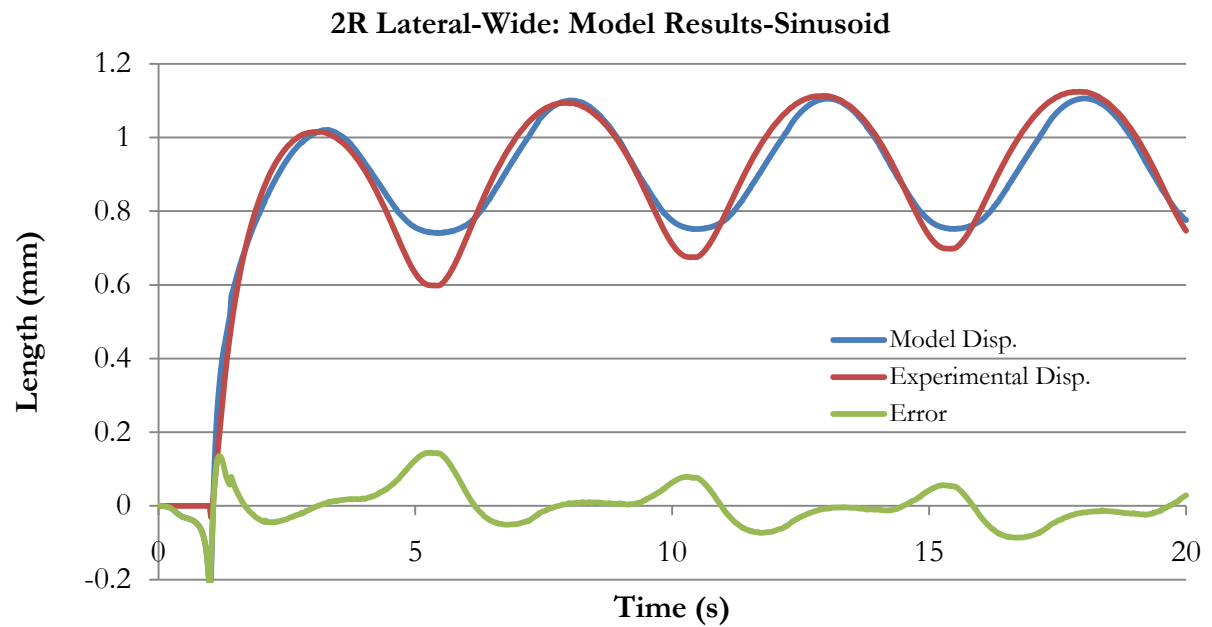


Figure 17. MB meniscus results for 2R Lateral-Wide

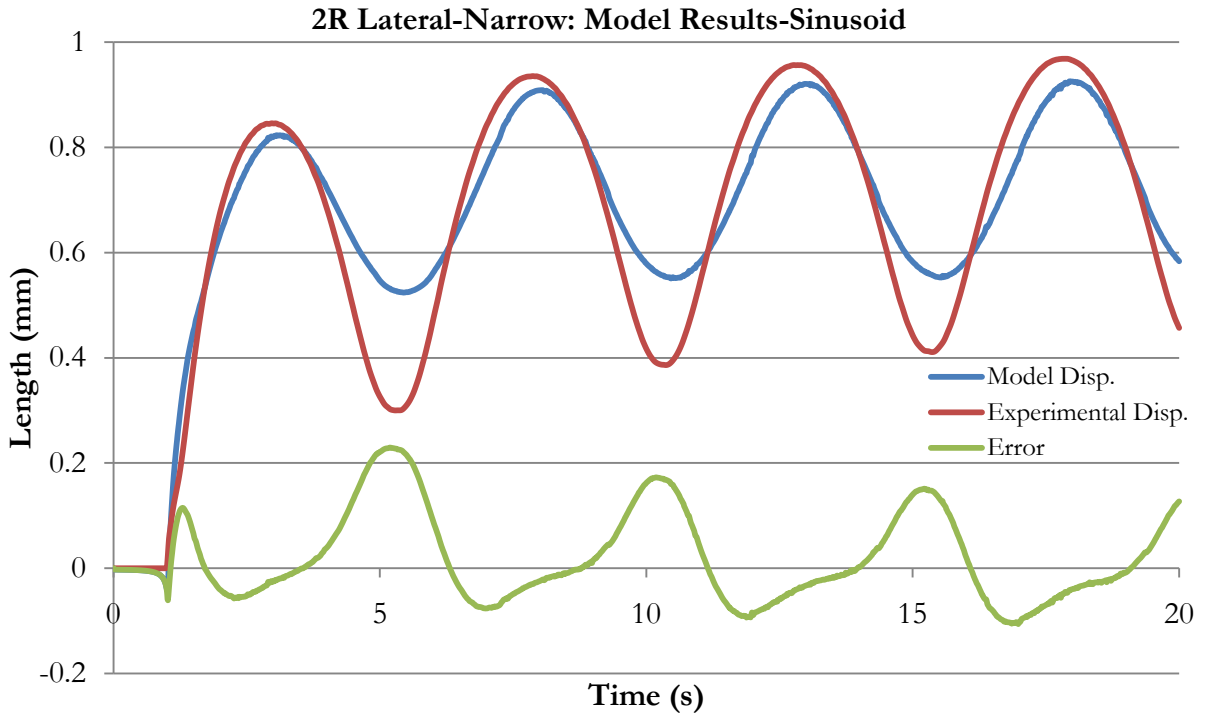


Figure 18. MB meniscus results for 2R Lateral-Narrow

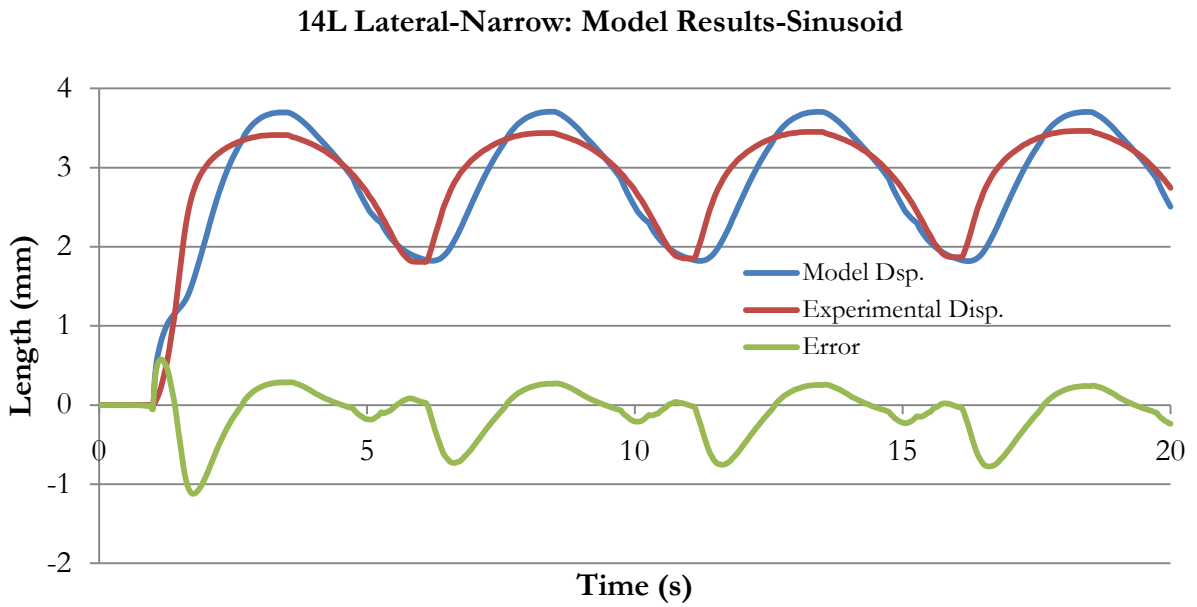


Figure 19. MB meniscus results for 14L Lateral-Narrow

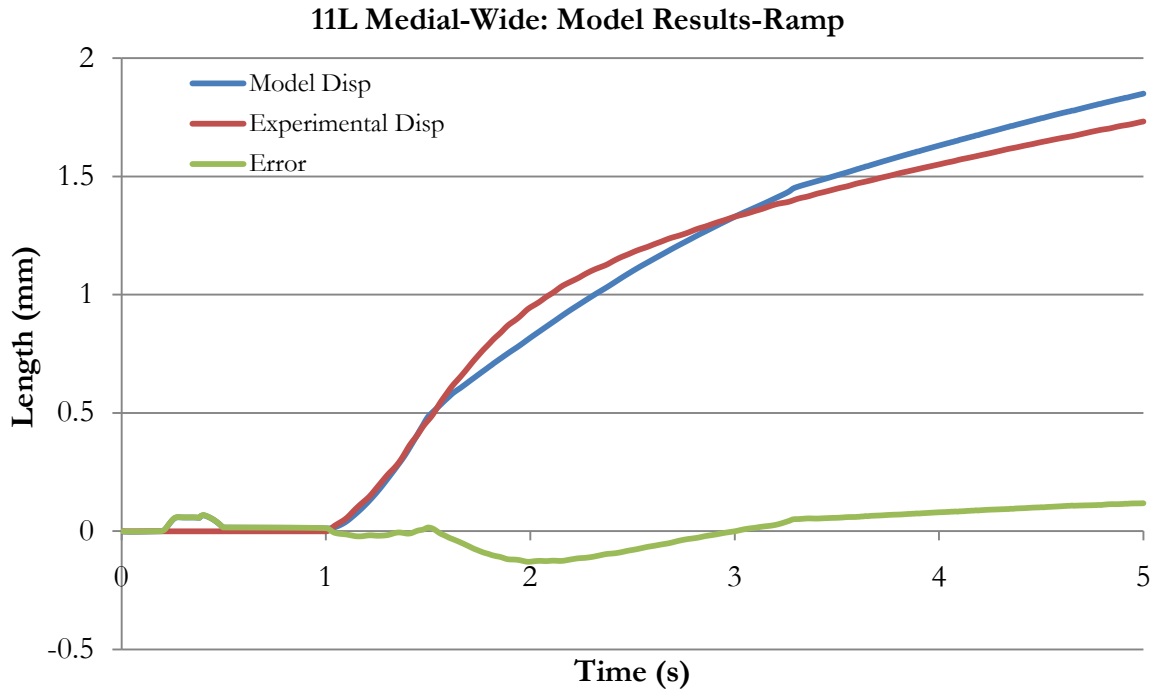


Figure 20. MB meniscus results for 11L Medial-Wide

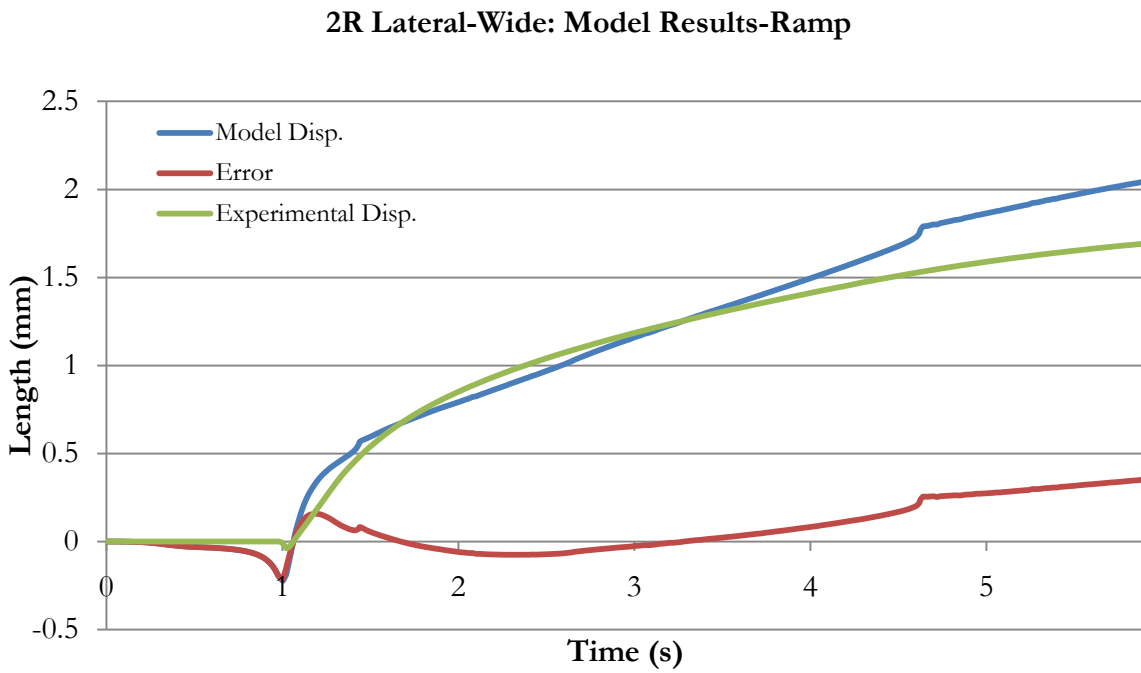


Figure 21. MB meniscus results for 2R Lateral -Wide

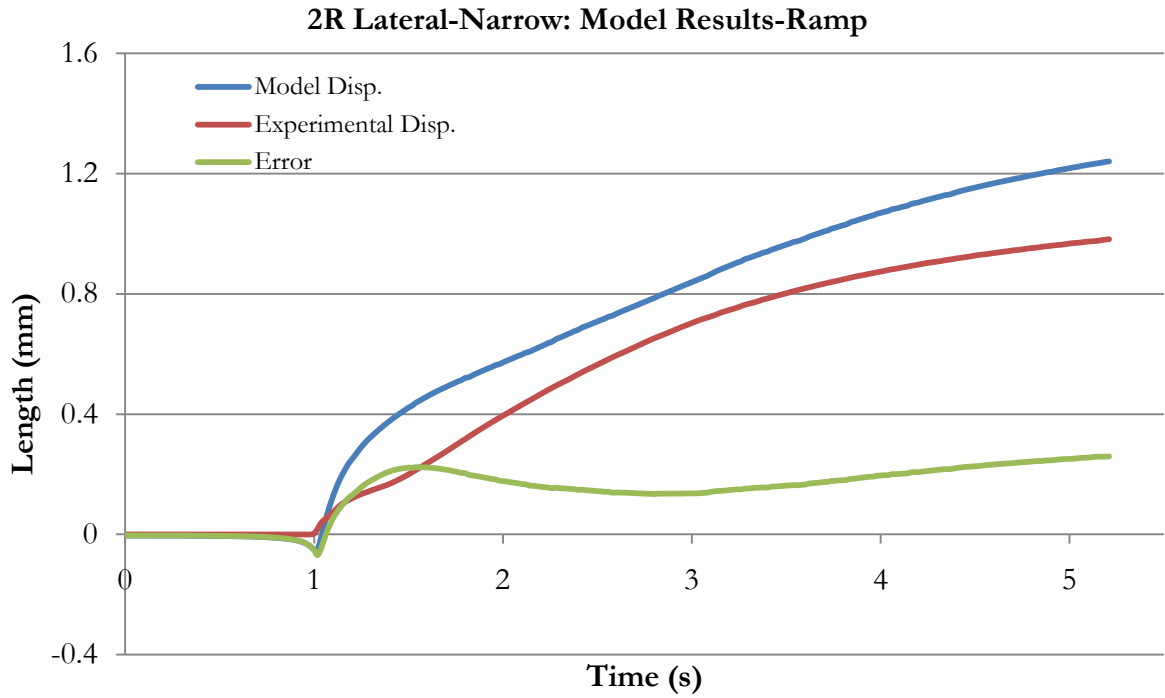


Figure 22. MB meniscus results for 2R Lateral-Narrow

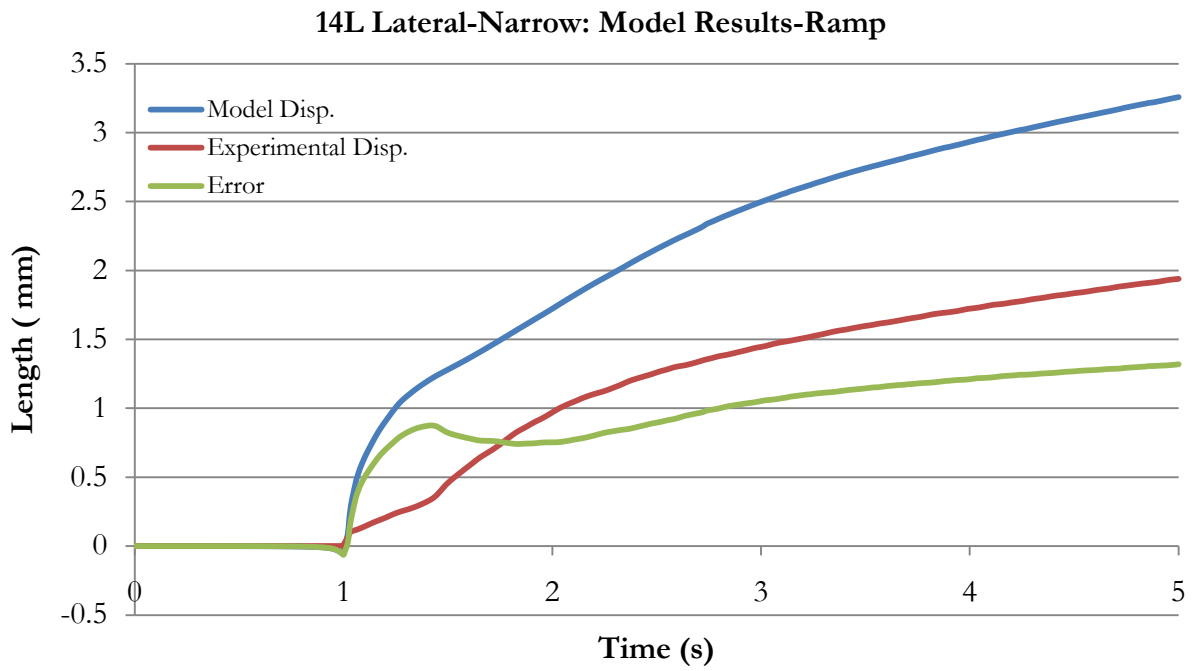


Figure 23. MB meniscus results for 14L Lateral-Narrow

For the 2R meniscus samples during ramp loading the simulation times used were 5.92s and 5.21s for the wide and narrow boundary conditions respectively.

#### 4.2.2 Cartilage Model.

Table 11. Cartilage indentation modeled Moduli of Elasticity

| Depth (mm) | G (N/mm <sup>2</sup> ) | R (mm) | Side    | h (mm) | E (N/mm <sup>2</sup> ) (Hertz) | E <sub>2</sub> (N/mm <sup>2</sup> ) (Waters) | E <sub>3</sub> (N/mm <sup>2</sup> ) (Hayes) |       |
|------------|------------------------|--------|---------|--------|--------------------------------|--|---|-------|
| 0.302      | 2.60                   | 1      | Lateral | 2.54   | 7.79                           | 5.31   | 6.03  |       |
| 0.129      | 9.28                   | 1      | Lateral | 2.34   | 27.85                          | 22.39  | 23.39                                       |       |
| 0.231      | 11.18                  | 2      | Lateral | 2.18   | 33.53                          | 16.57  | 22.70                                       |       |
| 0.528      | 3.25                   | 2      | Medial  | 2.56   | 9.74                           | 3.95   | 5.78  |       |
| 0.157      | 6.84                   | 1      | Medial  | 2.19   | 20.53                          | 15.21  | 16.66                                       |       |
| 0.204      | 13.51                  | 2      | Medial  | 2.14   | 40.52                          | 20.74  | 27.97                                       |       |
|            |                        |        |         | Avg    |                                | 23.33  | 14.03                                       | 17.09 |
|            |                        |        |         | Avg'   |                                | 30.61  | 18.73                                       | 22.68 |

' Denotes average excluding the two lowest values.

#### 4.2.3 Design of Experiments.

There were usually 4 stiffness variables that were consistently significant along with the initial displacement. The circumferential stiffness,  $K_{\theta}$ , and the torsional stiffness about the Z axis,  $T_z$ , were always significant to a  $p < .01$ . The radial stiffness,  $K_r$ , and the torsional stiffness,  $T_r$ , about the radial axis were usually significant to a  $p < .05$ . The initial displacement correction was very significant if the error was more than 0.5 mm but was usually insensitive inside of that range. Many of these terms had significant squared effects and interaction effects, but the damping ratios and the nonlinear length were consistently only significant in these effects. This indicates a strange dependence that is particularly hard to capture as it is highly dependent on nonlinearities that have not been accounted for.

## CHAPTER 5

### DISCUSSION

#### 5.1 Analysis of Experimental Results

The experimental performance is hard to quantify but were generally acceptable with normalized errors for the optimized trials being under 0.1mm. The goal of applying a semi-physiological loading to an intact meniscus has been accomplished. When looking at the experimental results by themselves the only noticeable area for improvements are in terms of consistency and repeatability. The fact that the load limit varied depending on the grip performance and the use of a second machine for the test of the 2R menisci provide some possibly unwanted effects. Not being able to attach the vises to the horn attachments made it so that some initial tension needed to be applied with forceps while the vices were tightened.

#### 5.2 Model Results

##### 5.2.1 Meniscus Performance

**DOE.** The DOE process greatly accelerated the optimization, particularly with the use of the integrated ADAMS/Insight package. Insight does not provide a fine level of control over the setup of the experiment, but the automation it provides as well as the built in solver for finding extrema to objective functions makes it an extremely valuable tool. Several of the DOE setups were analyzed in Minitab (Minitab, Inc. State College, PA) as well and provided identical answers pertaining to the significance of the effects. The process has several serious flaws relating to the multiplicity of near optimal solutions as well as the presence of local minima. The possibility of getting stuck in one of the minima is somewhat mitigated by the numerous combinations of small DOE's. The presence of many near optimal solutions is well

demonstrated by the interplay of the  $T_z$  and the  $K_0$  parameters. In many of the models an increase of one of these two parameters can be balanced by a corresponding decrease in the other. For example a doubling of one factor and corresponding reduction of the other parameter could produce model performance with error within 10% of the original solution. With additional optimization of some of the parameters this was seen to decrease to as little as 5%. This presents an extremely difficult situation for deciding on a reliable estimate for these two parameters. Performing the tests with two different width v-blocks was intended to help isolate the effects of parameter. However, currently they do not appear to be isolated. This is possible due to the presence of other variations between trials and there being enough difference between narrow and wide v-block values to confound any relationships. As mentioned, the *iDisp* value is another source of multiple minima.

The optimal values for the presented models seem to indicate that the shear/cross product terms are nearly inconsequential to the overall behavior in this semi-physiological loading and that the torsional stiffness about the circumference and the radii is similarly unimportant. This supports the theory that meniscus properties are heavily dominated by the collagen fiber orientation. The crucial material terms are in order of typically observed significance was  $K_b$ ,  $T_z$ ,  $K_p$ , DR, and  $X_r$ . As the nonlinear length tended to be a nonzero number at the located optima, it is assumed that the inclusion of this parameter improved the overall model performance. Compared to the results obtained for human meniscus from comparison to a linear FE by Guess et al. the values for the significant stiffnesses are 2-4 times as stiff and the less significant stiffness are close to two orders of magnitude lower. Some contribution to this increased stiffness may be due to the introduction of the nonlinear  $K_0$  but this is a much larger effect than anticipated. There are two large differences that should account for the majority of the remaining discrepancy. First and foremost is the fact that a canine meniscus and

a human meniscus may differ to some extent chemically, morphologically, or in terms of composition. Distribution of fibers, fiber sizes, and the distribution of chemical species would be expected to cause significant differences as these are the chief differences between bone, cartilage, and ligamentous tissue. Supporting this is the fact that it has been demonstrated that the human and canine meniscus have significantly different aggregate modulus (Sweigart et al. 2004). The second likely source for this discrepancy is differences that occur purely in the modeling format. A good example of this is the scale of the model; the 14L lateral canine menisci measured 19.5 mm across the horns whereas a small human lateral meniscus measures 27.5 mm. The maximum distraction for the human FE model was about 5.4mm mm whereas the typical distraction of the canine experiments was less than 3mm. It is unknown how reducing the scale of the model would affect its overall behavior, but it is known that shape is a significant source of nonlinearity in the model.

**General meniscus model performance.** The overall performance of using a rigid MB model to represent a deformable tissue was excellent. Visually the technique demonstrated the expected stretching, sliding, wrapping, and twisting behaviors. In general it can be seen that the model performance lagged slightly and did not recover as quickly to rapid decreases in load (Figures 16 through 23). The errors for the sinusoidal profiles were in the 0.0523 to 0.328 mm range with an average of 0.136 mm. This a considerable improvement over the values determined from the adaptation of Guess et al. 2010 which had a range of 0.199 to 1.75mm and an average of 0.843 mm. Ramp performance did not exhibit as significant an improvement but still averaged 0.329mm with a range of 0.0670 to 0.910 mm, down from 0.572mm and 0.288 to 0.818mm. This improvement indicates that these models perform adequately but there is room for further improvement in the technique and the collection of usable experimental data.



The acceptable modeling of the ramps validates the values selected for each meniscus model. The 14L lateral meniscus exhibits the worst RMS error but with two likely explanations. The 14L meniscus at times exhibited an artificial behavior where the edge of a meniscus section would catch on the corner of the v-block. This is a purely artificial error as no organic shape would exhibit this shape. Additionally the 14L meniscus exhibits the largest deformation and the 2R meniscus test the lowest. As these menisci represent the highest and lowest RMS and  $K$  values this indicates some tendency of the material properties to vary depending the expected deformation range.

The fact that several of the property values exhibit large standard of deviations (over 100% of the mean) can likely be explained in several manners. First it is important to note that with this small of a sample size none of the values are beyond 1.49 times the standard of deviation from the mean for a given parameter. This makes it impractical to properly classify an outlier. The 2R lateral wide meniscus values for  $DR$  and  $K_\theta$  and the 2R lateral narrow value for  $K_z$  are the most suspect values. The  $iDisp$  parameter exhibits a similar spread. This is expected as it reflects a compensation for human error in experimentation and not a material property. For this reason the  $iDisp$  variable is considered a per model parameter and no nominal value is given. Similarly no nominal value for  $X_j$  is given as while it is a material property it is partially dependent on the number of meniscus segments. The most straight forward explanation for the spread in material properties is that the material properties will exhibit some variation between individuals. One would expect this particularly in a species as morphologically diverse as canines. Other possibilities include the uncertainty in the orientation of the meniscus about the v-block along the  $Z$ -axis. Additional factors that could account for this discrepancy include complications with the DOE. It should also be noted that the  $X_k$  should be highly dependent

on the segmentation process as it is expected to depend on the number of segments within the flexible multibody tissue.

Initially, the testing with two different sized V-blocks was intended to provide insight into this issue by providing two separate boundary conditions on the same meniscus. Unfortunately there was not enough information to align each of the two models separately and accurately so there are additional boundary related initial conditions that are unknown, this confounds the result and makes it impossible to determine the effect of just the v-block size. Additionally, this problem is exacerbated by the holes in the data due to trials involving slippage of the sample. Overall a nominal average value was determined and is displayed in Table 8. The plain mean is likely the most distorted by the extreme outliers and is considered the most suspect. The average of the mean and median and the median should be considered more robust values. This is generally supported by rerunning all four meniscus models with the three parameter sets. The 0.620 mm RMS value for the average of the mean and median values supports this statement. If outliers could be determined with confidence it is possible the median values would produce the lowest errors.

### **5.3 Improvements**

If this was to be redone the meniscus test would be done more easily with improvements to the experimental set up and to the modeling procedure.

Experimentally the process would have been much more successful with better quality MRI's particularly with respect to decreasing the slice thickness. When the joint was disarticulated it would have helped the procedure if more of the horn attachments had been left intact, this would have made it possible to clamp the vices to the horn attachments as originally intended instead of to the edges of the meniscus proper. This requires the addition of the horn

attachments to the MB model but would lend itself to improved consistence in loading that can be applied without slippage. To provide more alignment information the vertical portion of the fixture could be made thinner to allow a photo along the Z-axis to show the anterior and posterior portions of the meniscus being tested. This would allow for some alignment about the z axis of the menisci. A further step to improve results would have been to perform all of the experiments in a saline bath to encourage full material recovery after the dynamic tests.

A new field element library was written for this procedure to include a nonlinear circumferential tension. This could be expanded to include other model improvements. One possibility would be to separate the damping ratios for the circumferential stiffness and the axial torsional stiffness. This may be beneficial as the ratio was artificially limited to a 0.2 value to benefit the simulation process as there was a risk of instability below this. It is quite likely that a lower ratio for the two dominate stiffnesses would have improved the error but not affected the simulation quality. It may even be possible to replace the simplified viscous damping with a viscoelastic parameter that more accurately captures the biological tissues behavior. This would be most easily done by implementing a Kelvin, Voigt, or Standard Viscoelastic model that is typically represented by a set of series or parallel springs and dashpots. The contact parameters could benefit from similar improvements. Some method of indentation or compression between platens could be used to produce an estimate of physiological contact parameters. This could also be improved by customizing the ADAMS contact subroutine to include viscoelastic effects. Other dramatic changes could be to implement segmentation in the radial direction as well.

## CHAPTER 6

### CONCLUSION & FUTURE WORK

The overall objective of this study to demonstrate the capability of the multibody method to capture the flexible behavior of soft biological tissue was accomplished with a reasonable level of success. The largest qualifier to this statement is that the optimum parameters for different experimental trials vary significantly and that there is little agreement between separate meniscus tests. The experimental portion of this study is partially to blame for this as it had too many unknowns in the initial conditions of the meniscus being tested. An example of the unknown initial conditions would be the preload/strain that had been applied to each sample. In the process the testing no known preload was applied; however, placing the meniscus in the v-blocks was difficult due to the small scale and confined space for placing the meniscus. Additionally the meniscus horns were pulled into the holding vices using tweezers, while a significant force preload would be unexpected, it is possible that due to relaxation of the material, some prestrain was present after this operation. Unfortunately the modeling method can also be responsible for the wide parameter variation due to the complex interactions of some of the stiffness parameters and the multiple near optimal solutions. To have confidence in the parameters determined from this procedure either a larger sample size allowing the identification of outliers, or a procedure that allows the initial conditions to be modeled more exactly is needed.

Future work includes implementing the improvements mentioned in section 5.3 and finishing the development of the cartilage indentation data. The improvements in the meniscus modeling focus on removing the unknown initial conditions of the experimental apparatus and improvements to the MB modeling technique as it applies to biological tissues. The cartilage

indentation data is currently being explored as a calibration for a similar MB model. The cartilage MB model consists of the segmented geometries bonded rigidly to a substrate and then the creation of contacts to the other articular surfaces. The primitive modeling done here demonstrates the sensitivity of the behavior to the cartilage thickness (Table 11). As this is a parameter that currently does not affect the contact model a reasonable average value must be determined or a modified contact algorithm must be created. Currently the experimental data and the MB model are being compared to a FE model in the attempts to create a surrogate model that can determine internal cartilage parameters based off of MB model inputs.

## APPENDIX A

The nonlinear field element formulation as written for compiling into an ADAMS dll:

```
#include "slv_c_utils.h"
#include <math.h>

adams_c_Fiesub    Fiesub;

void Fiesub(const struct sAdamsField* fie, double time,
            double* disp, double* velo, int dflag ,int iflag,
            double* field, double* dfddis, double* dfdvel)
{
double Er = fie->PAR[9];
double Cr = fie->PAR[10];
double sign = 1;
/*
    fie      sAdamsField structure:
            int ID      Identifier of calling FIELD statement
            int Nfie->PAR  Number of passed fie->PARAMeters
            double fie->PAR  Array of passed statement fie->PARAMeters
            int I      Field I Marker
            int J      Field I Marker
time      Current time
disp      Array of I with respect to J displacements  (X,Y,Z,a,b,c)
velo      Array of I with respect to J velocities
dflag     Differencing flag
iflag     Initialization pass flag
field     Array of field values
dfddis    displacement fie->PARTIAL derivatives
dfdvel    Velocity fie->PARTIAL derivatives
the PAR array consists of user inputed terms
The X direction corresponds to the circumferential (Theta) direction
The Y direction the radial (r), and the Z the axial (z)
PAR[0] is the [1,1] term of the stiffness matrix in N/mm, likewise:
PAR[1] is the [1,2] and [2,1]
PAR[2] is the [1,3] and [3,1]
PAR[3] is the [2,2]
PAR[4] is the [2,3] and [3,2]
PAR[5] is the [3,3]
PAR[6] is the [4,4]
PAR[7] is the [5,5]
PAR[8] is the [6,6]
PAR[9] is the nonlinear length in mm
PAR[10] is the damping ratio term
*/
/* --- Calculate field component forces -----*/
/* Note: Velocity effects represented as Cr*(the stiffness
parameters)*velocity */
/* X translation field force, piecewise formulation */

    if (disp[0] < 0)
        sign = -1;
    else
        sign = 1;
```

```

        if (fabs(displ[0]) < (2*Er))
        {
            field[0] = - fie->PAR[0] * .25*sign* pow(fabs(displ[0]),2)/Er-
fie->PAR[0]*Cr*(velo[0])
                                - fie->PAR[1] * displ[1]-fie-
>PAR[1]*Cr*(velo[1])
                                - fie->PAR[2] * displ[2]-fie-
>PAR[2]*Cr*(velo[2]);
        }

        else
        {
            field[0] = - fie->PAR[0] *(displ[0] - sign* Er)-fie-
>PAR[0]*Cr*(velo[0])
                                - fie->PAR[1] * displ[1]-fie-
>PAR[1]*Cr*(velo[1])
                                - fie->PAR[2] * displ[2]-fie-
>PAR[2]*Cr*(velo[2]);
        }
/* Y translation field force */

        {
            field[1] = - fie->PAR[3] *(displ[1])-fie->PAR[3]*Cr*(velo[1])
                                - fie->PAR[1] * displ[0]-fie-
>PAR[1]*Cr*(velo[0])
                                - fie->PAR[4] * displ[2]-fie-
>PAR[4]*Cr*(velo[2]);
        }
/* Z translation field force */

        {
            field[2] = - fie->PAR[5] *(displ[2])-fie->PAR[5]*Cr*(velo[2])
                                - fie->PAR[2] * displ[0]-fie-
>PAR[2]*Cr*(velo[0])
                                - fie->PAR[4] * displ[1]-fie-
>PAR[4]*Cr*(velo[1]);
        }

/* --- Calculate field component torques ----- */
/* X rotational field torque (displacement a)*/

        field[3] = - fie->PAR[6] *displ[3]-fie->PAR[6]*Cr*(velo[3]);

/* Y rotational field torque (displacement b)*/

        field[4] = - fie->PAR[7] *displ[4]-fie->PAR[7]*Cr*(velo[4]);

/* Z rotational field torque (displacement c) */

        field[5] = - fie->PAR[8] *displ[5]-fie->PAR[8]*Cr*(velo[5]);
/*
--- Assign returned fie->PARTIAL derivatives with -----
respect to displ if this is a differencing pass
*/
        if ( dflag ) {

/* Initialize all derivatives to zero. */

```

```

    int i,j;
    for( j=0; j<6; j++){
        for( i=0; i<6; i++){
            dfddis[j*6+i] = 0.0;
            dfdvel[j*6+i] = 0.0;
        }
    }
/* Assign displacement partials for X force  dfddis[2*6+0] is partial of
Fx with respect to disp Z */

    if (fabs(displ[0]) < (2*Er))

        dfddis[0*6+0] = - fie->PAR[0] * .5* fabs(displ[0])/Er;

    else

        dfddis[0*6+0] = - fie->PAR[0];

        dfddis[1*6+0] = - fie->PAR[1];
        dfddis[2*6+0] = - fie->PAR[2];

/* Assign displacement partials for Y force */

        dfddis[0*6+1] = - fie->PAR[1];
        dfddis[1*6+1] = - fie->PAR[3];
        dfddis[2*6+1] = - fie->PAR[4];
/* Assign displacement partials for Z force */

        dfddis[0*6+2] = - fie->PAR[2];
        dfddis[1*6+2] = - fie->PAR[4];
        dfddis[2*6+2] = - fie->PAR[5];

/* X torque displacement partial */
        dfddis[3*6+3] = -fie->PAR[6];
/* Assign displacement partials for Y torque */
        dfddis[4*6+4] = -fie->PAR[7];
/* Z torque displacement partials */
        dfddis[5*6+5] = -fie->PAR[8];
/* --- THE X force partial derivatives with respect to VELO --- */
        dfdvel[0*6+0] = -fie->PAR[0]*Cr;
        dfdvel[1*6+0] = - fie->PAR[1]*Cr;
        dfdvel[2*6+0] = - fie->PAR[2]*Cr;
/* Y force velocity partials */
        dfdvel[0*6+1] = -fie->PAR[1]*Cr;
        dfdvel[1*6+1] = - fie->PAR[3]*Cr;
        dfdvel[2*6+1] = - fie->PAR[4]*Cr;
/* Assign velo partials for Z force */
        dfdvel[0*6+2] = -fie->PAR[2]*Cr;
        dfdvel[1*6+2] = - fie->PAR[4]*Cr;
        dfdvel[2*6+2] = - fie->PAR[5]*Cr;
/* X torque displacement partials */
        dfdvel[3*6+3] = -fie->PAR[6]*Cr;
/* Assign displacement partials for Y torque */
        dfdvel[4*6+4] = -fie->PAR[7]*Cr;
/* Assign displacement partials for z torque */
        dfdvel[5*6+5] = -fie->PAR[8]*Cr;
    }
}

```



## APPENDIX B

The scripts shown here were originally written by Mohammad Kia for the Guess et al. 2010 project. They have been modified here with his permission. The ADAMS macro used to generate the segmented meniscus geometries, the macro to connect the meniscus segments with field elements, and the macro to generate contacts between a MB meniscus and another geometry are included here.

### Macro\_div2

```
!$DICE_MOD:T=Model
!$DICE_PAR:T=part
!$DICE_GEO:T=geometry
!
!
!$CELLSIDE:T=Integer

    !$RMAX:T=real

        !$ZSTART:T=integer
        !$ZEND:T=integer
!$X_CENT:T=real
!$Y_CENT:T=real
!$INI_ANG:T=integer
!
!
!!!! DICE_MOD,DICE_PAR, and DICE_GEO are the model, part and geometry
names of the
!!!! meniscus to be segmented.  CELLSIDE is the wedge angle desired for
each
!!!! segment.  RMAX, ZSTART, ZEND, define the size and Z position of the
intersecting
!!!! cylinder that generates the wedge.  X_CENT and Y_CENT are the
cylinders X and Y
!!!! position.  INI_ANG is the angle from the X axis that the first wedge
will be
!!!! generated from.  It is important to note that for proper operation
the ADAMS
!!!! models orientation must be set to body 313.
variable create variable_name=$_self.r_cells integer_value=(360/$CELLSIDE)
!
!
!
variable create variable_name=$_self.marker_name
string_Value=(UNIQUE_NAME("INT_MRK"))
variable create variable_name=$_self.cylinder_name
string_Value=(UNIQUE_NAME("INT_CYL"))
variable create variable_name=$_self.part_name
string_Value=(UNIQUE_NAME("INT_PAR"))
variable create variable_name=$_self.geo_name
string_Value=(UNIQUE_NAME("INT_GEO"))
variable create variable_name=$_self.csg_name
string_Value=(UNIQUE_NAME("CSG_CELL"))
!
```

```

variable create variable_name=$_self.con_f_name
string_Value=(UNIQUE_NAME("CON_F_ELE"))
variable create variable_name=$_self.gcon_name
string_Value=(UNIQUE_NAME("GCON_FOR"))

variable create variable_name=$_self.con_t_name
string_Value=(UNIQUE_NAME("CON_T_ELE"))
variable create variable_name=$_self.gcon_t_name
string_Value=(UNIQUE_NAME("GCON_T_FOR"))
!
variable create variable_name=$_self.color_flag integer_value=1
variable create variable_name=$_self.color_row_flag integer_value=1
!
!
for variable_name=$_self.r_count start_value=0 increment_value=1
end_value=(EVAL($_self.r_cells-1))
!
! Checkerboard colouring: The start colour for each row must alternate:
if condition=($_self.color_row_flag==1)
variable set variable_name=$_self.color_row_flag integer_value=0
else
variable set variable_name=$_self.color_row_flag integer_value=1
end ! if
variable set variable_name=$_self.color_flag
integer_value=(EVAL($_self.color_row_flag))
!
!
!
! Create Cylinder :
part create rigid_body name_and_position
part_name=.( $DICE_MOD ).(EVAL($_self.part_name))
!
marker create
marker=.( $DICE_MOD ).(EVAL($_self.part_name)).(EVAL($_self.marker_name)) &
location=( $X_CENT ),( $Y_CENT ),( $ZSTART ) &
orientation=0,0,( $INI_ANG+(EVAL($_self.r_count))*$CELLSIDE)
geometry create shape cylinder&

cylinder_name=.( $DICE_MOD ).(EVAL($_self.part_name)).(EVAL($_self.cylinder_
name)) &
length=(( $ZEND )-( $ZSTART )) &
radius=( $RMAX )&
angle=( $CELLSIDE )&

center_marker=.( $DICE_MOD ).(EVAL($_self.part_name)).(EVAL($_self.marker_na
me))
!!!!!!!!!!!!!!!!!!!!!!!!!!!!!!!!!!!!!!!!!!!!!!!!!!!!!!!!!!!!!!!!!!!!!!!!!!!!!!
!!!!!!!!!!!!!!!!!!!!!!!!!!!!!!!!!!!!!!!!!!!!!!!!!!!!!!!!!!!!!!!!!!!!!!!!!!!!!!
group modify group=SELECT_LIST obj=.( $DICE_MOD ).(EVAL($_self.part_name))
expand_groups=no
!mdi modify_macro
if condition = 1
part modify rigid mass_properties &
part_name = .( $DICE_MOD ).(EVAL($_self.part_name)) &
&
&
&

```

```

&
&
&
&
&
&
density = ($DICE_MOD.DV_Menisci_Density) &

end!if
!
!!!!!!!!!!!!!!!!!!!!!!!!!!!!!!!!!!!!!!!!!!!!!!!!!!!!!!!!!!!!!!!!!!!!!!!!!!!!!!
!!!!!!!!!!!!!!!!!!!!!!!!!!!!!!!!!!!!!!!!!!!!!!!!!!!!!!!!!!!!!!!!!!!!!!!!!!!!!!
!
!Create a new copy of the input geometry:
    geometry copy geometry_name=$DICE_GEO
new_geometry_name=(EVAL($_self.geo_name))
!
! Intersect the copy of the input geometry, and the cylinder from the
previous step:
    geometry create shape csg
csg_name=.( $DICE_MOD).(EVAL($_self.part_name)).(EVAL($_self.csg_name)) &
    base_object=.(EVAL($_self.cylinder_name)) &
    object=.(EVAL($_self.geo_name)) &
    type=intersection
!
! Detect if the intersect operation failed (i.e. no geometry created).
    if condition=(DB_EXISTS($_self.csg_name)==0)
        ! If operation failed, delete the unused construction geometry:
        part delete part_name=.( $DICE_MOD).(EVAL($_self.part_name))
        geometry delete
geometry_name=.( $DICE_MOD).(EVAL($_self.part_name)).(EVAL($_self.block_name))
        geometry delete
geometry_name=.( $DICE_MOD).(EVAL($_self.part_name)).(EVAL($_self.geo_name))
    )
        marker delete
marker_name=.( $DICE_MOD).(EVAL($_self.part_name)).(EVAL($_self.marker_name))
    )
    end ! if
!!!!!!!!!!!!!!!!!!!!!!!!!!!!!!!!!!!!!!!!!!!!!!!!!!!!!!!!!!!!!!!!!!!!!!!!!!!!!!
!!!!!!!!!!!!!!!!!!!!!!!!!!!!!!!!!!!!!!!!!!!!!!!!!!!!!!!!!!!!!!!!!!!!!!!!!!!!!!
!!!!!!!!!!!!!!!!!!!!!!!!!!!!!!!!!!!!!!!!!!!!!!!!!!!!!!!!!!!!!!!!!!!!!!!!!!!!!!
!   Replace the CSG geometries with identical parasolid geometries
!!!!!!!!!!!!!!!!!!!!!!!!!!!!!!!!!!!!!!!!!!!!!!!!!!!!!!!!!!!!!!!!!!!!!!!!!!!!!!
!!!!!!!!!!!!!!!!!!!!!!!!!!!!!!!!!!!!!!!!!!!!!!!!!!!!!!!!!!!!!!!!!!!!!!!!!!!!!!
!
    group modify group=SELECT_LIST
obj=.( $DICE_MOD).(EVAL($_self.part_name)).(EVAL($_self.csg_name))
expand_groups=no

    file parasolid write &
    file_name = "ParS_Cell" &
    type = binary &
    &
    &
    &
    part_name = .( $DICE_MOD).(EVAL($_self.part_name))

```

```

!
    geometry delete
geometry_name=.( $DICE_MOD ).( EVAL( $_self.part_name ) ).( EVAL( $_self.csg_name )
)

    file parasolid read &
    file_name = "ParS_Cell.xmt_bin" &
    type = BINARY &
    &
    part_name = .( $DICE_MOD ).( EVAL( $_self.part_name ) ) &
    &
    orientation = 0.0, 0.0, 0.0 &
    relative_to = .( $DICE_MOD ).( EVAL( $_self.part_name ) ) &
    explode_assemblies = no

!
!!!!!!!!!!!!!!!!!!!!!!!!!!!!!!!!!!!!!!!!!!!!!!!!!!!!!!!!!!!!!!!!!!!!!!!!!!!!!!!!!!!!!!!!!!!!!!!!!!!!!!!!!!!!!!!!!!!!!!!!
!!!!!!!!!!!!!!!!!!!!!!!!!!!!!!!!!!!!!!!!!!!!!!!!!!!!!!!!!!!!!!!!!!!!!!!!!!!!!!!!!!!!!!!!!!!!!!!!!!!!!!!!!!!!!!!!!!!!!!!!
!
!!!!!!!!!!!!!!!!!!!!!!!!!!!!!!!!!!!!!!!!!!!!!!!!!!!!!!!!!!!!!!!!!!!!!!!!!!!!!!!!!!!!!!!!!!!!!!!!!!!!!!!!!!!!!!!!!!!!!!!!
!!!!!!!!!!!!!!!!!!!!!!!!!!!!!!!!!!!!!!!!!!!!!!!!!!!!!!!!!!!!!!!!!!!!!!!!!!!!!!!!!!!!!!!!!!!!!!!!!!!!!!!!!!!!!!!!!!!!!!!!
!
!
!
! Apply 'checkerboard' colour to cell:
    if condition=( $_self.color_flag==1)
        variable set variable_name=$_self.color_flag integer_value=0
        if condition=(DB_EXISTS($_self.csg_name))
            geometry attributes
geometry_name=.( $DICE_MOD ).( EVAL( $_self.part_name ) ).( EVAL( $_self.csg_name )
) color=red
        end ! if
    else
        variable set variable_name=$_self.color_flag integer_value=1
        if condition=(DB_EXISTS($_self.csg_name))
            geometry attributes
geometry_name=.( $DICE_MOD ).( EVAL( $_self.part_name ) ).( EVAL( $_self.csg_name )
) color=blue
        end ! if
    end ! if

!!!!!!!!!!!!!!!!!!!!!!!!!!!!!!!!!!!!!!!!!!!!!!!!!!!!!!!!!!!!!!!!!!!!!!!!!!!!!!!!!!!!!!!!!!!!!!!!!!!!!!!!!!!!!!!!!!!!!!!!
!!!!!!!!!!!!!!!!!!!!!!!!!!!!!!!!!!!!!!!!!!!!!!!!!!!!!!!!!!!!!!!!!!!!!!!!!!!!!!!!!!!!!!!!!!!!!!!!!!!!!!!!!!!!!!!!!!!!!!!!
!!
!
!!!!!!!!!!!!!!!!!!!!!!!!!!!!!!!!!!!!!!!!!!!!!!!!!!!!!!!!!!!!!!!!!!!!!!!!!!!!!!!!!!!!!!!!!!!!!!!!!!!!!!!!!!!!!!!!!!!!!!!!
!!!!!!!!!!!!!!!!!!!!!!!!!!!!!!!!!!!!!!!!!!!!!!!!!!!!!!!!!!!!!!!!!!!!!!!!!!!!!!!!!!!!!!!!!!!!!!!!!!!!!!!!!!!!!!!!!!!!!!!!
!
!
!
! Update the object name strings to new unique values:
    variable set variable_name=$_self.marker_name
string_value=(UNIQUE_NAME("INT_MRK"))
    variable set variable_name=$_self.cylinder_name
string_value=(UNIQUE_NAME("INT_CYL"))
    variable set variable_name=$_self.part_name
string_value=(UNIQUE_NAME("INT_PAR"))
    variable set variable_name=$_self.geo_name
string_value=(UNIQUE_NAME("INT_GEO"))

```

```
        variable set variable_name=$_self.csg_name
string_Value=(UNIQUE_NAME("CSG_CELL"))
end ! for
!
!!!!!!!!!!!!!!!!!!!!!!!!!!!!!!!!!!!!!!!!!!!!!!!!!!!!!!!!!!!!!!!!!!!!!!!!!!!!
!!!!!!!!!!!!!!!!!!!!!!!!!!!!!!!!!!!!
!
!!!!!!!!!!!!!!!!!!!!!!!!!!!!!!!!!!!!!!!!!!!!!!!!!!!!!!!!!!!!!!!!!!!!!!!!!!!!
!!!!!!!!!!!!!!!!!!!!!!!!!!!!!!!!!!!!
!
Part delete part_name=$DICE_PAR
!
defaults attributes icon_visibility="off"
view manage modify render=sshaded
```

## Macro\_lfie2

```
!$DICE_MOD:T=Model
!$CELLSIDE:T=Integer
!$START_PAR:T=Integer
!$LAST_PAR:T=Integer
!$INI_ANG:T=Integer
!$FIE_ANG:T=Integer
!$X_CENT:T=real
!$Y_CENT:T=real
!$Z_CENT:T=real
!
!!!! DICE_MOD is the model name that contains a segmented meniscus that
needs
!!!! field element connections. CELLSIDE is the wedge angle used for each
!!!! segment. As the Macro_div2 macro names the new parts consistently
only the
!!!! numerical suffix of the first and last part are needed (START_PAR,
and LAST_PAR)
!!!! X_CENT, Y_CENT, and Z_cen define the center of rotation for the
field elements
!!!! position. INI_ANG is the angle from the X axis of the first wedge
FIE_ANG is
!!!! INI_ANG plus 90 degrees
!!!! It is important to note that for proper operation the ADAMS
!!!! models orientation must be set to body 313.
variable create variable_name=$_self.REF_name
string_Value=(UNIQUE_NAME("REF_MAR"))
!
!
variable create variable_name=$_self.r_field integer_value=(360/$CELLSIDE)
!
!
variable create variable_name=$_self.field_marker_name
string_Value=(UNIQUE_NAME("INT_FIE_MRK"))
variable create variable_name=$_self.field_name
string_Value=(UNIQUE_NAME("INT_FIE"))
!
!
!
variable create variable_name=ip integer_value=$START_PAR
variable create variable_name=jp integer_value=($START_PAR+1)
variable create variable_name=kp integer_value=1
!
! CREATE COORDINATE SYSTEM
marker create marker=.(($DICE_MOD).ground.(EVAL($_self.REF_name)) location
= ($X_CENT),($Y_CENT),($Z_CENT)
orientation=($INI_ANG+(EVAL(kp))*$CELLSIDE), 0.0, 0.0
!
!
variable create variable_name=ra
real_value=(( (Eval(DM((EVAL("INT_PAR_"//ip).cm),
(EVAL($_self.REF_name)))))+(Eval(DM((EVAL("INT_PAR_"//jp).cm),
(EVAL($_self.REF_name))))))/2)
variable create variable_name=hi
real_value=(( (Eval(DZ((EVAL("INT_PAR_"//ip).cm),
```

```

(EVAL($_self.REF_name)),(EVAL($_self.REF_name)))))+(Eval(DZ((EVAL("INT_PAR
_">//jp).cm), (EVAL($_self.REF_name)),(EVAL($_self.REF_name)))))/2)
!
for variable_name=$_self.f_count start_value=1 increment_value=1
end_value=(EVAL($_self.r_field-1))
!!!!!!!!!!!!!!!!!!!!!!!!!!!!!!!!!!!!!!!!!!!!!!!!!!!!!!!!!!!!!!
entity attributes &
  entity_name      = (EVAL($_self.REF_name)) &
  type_filter      = Marker &
  visibility       = off &
  name_visibility  = off &
  &
  entity_scope     = all_color &
  size             = 1 &
  &
  transparency     = 0
!
!!!!!!!!!!!!!!!!!!!!!!!!!!!!!!!!!!!!!!!!!!!!!!!!!!!!!!!!!!!!!!
!
!
! CREATE FIELD
undo begin

!

marker create
marker=.( $DICE_MOD).(EVAL("INT_PAR_"//ip)).(EVAL($_self.field_marker_name)
) location
=(LOC_RELATIVE_TO({(LOC_CYLINDRICAL((Eval(ra)),0,(Eval(hi))))},(EVAL($_sel
f.REF_name))))
orientation=( $FIE_ANG+(EVAL($_self.f_count))*$CELLSIDE),0.0,0.0
marker create
marker=.( $DICE_MOD).(EVAL("INT_PAR_"//jp)).(EVAL($_self.field_marker_name)
) location
=(LOC_RELATIVE_TO({(LOC_CYLINDRICAL((Eval(ra)),0,(Eval(hi))))},(EVAL($_sel
f.REF_name))))
orientation=( $FIE_ANG+(EVAL($_self.f_count))*$CELLSIDE),0.0,0.0
  force create element_like field &
  field_name=.( $DICE_MOD).(EVAL($_self.field_name )) &

i_marker_name=.( $DICE_MOD).(EVAL("INT_PAR_"//ip)).(EVAL($_self.field_marke
r_name)) &

j_marker_name=.( $DICE_MOD).(EVAL("INT_PAR_"//jp)).(EVAL($_self.field_marke
r_name)) &
!      stiffness_matrix= &
!      ($DICE_MOD.DV_LKXX),($DICE_MOD.DV_LKXY),($DICE_MOD.DV_LKXZ),0,0,0,
&
!      ($DICE_MOD.DV_LKXY),($DICE_MOD.DV_LKYY),($DICE_MOD.DV_LKYZ),0,0,0,
&
!      ($DICE_MOD.DV_LKXZ),($DICE_MOD.DV_LKYZ),($DICE_MOD.DV_LKZZ),0,0,0,
&
!      0,0,0,($DICE_MOD.DV_LTXX),0,0, &
!      0,0,0,0,($DICE_MOD.DV_LTYX),0, &
!      0,0,0,0,0,($DICE_MOD.DV_LTZZ) &
!      damping_ratio = ($DICE_MOD.DV_DR) &

```

```

        user_function =
(DV_LKXX),(DV_LKXY),(DV_LKXZ),(DV_LKYY),(DV_LKYZ),(DV_LKZZ),(DV_LTXX),(DV_
LTTY),(DV_LTZZ),(DV_Er),(DV_DR)  &
        routine = "fiesub_nlin64::"
        ! comments=""
mdi graphic_force object=.( $DICE_MOD).(EVAL($_self.field_name )) type=1
group modify group=SELECT_LIST object=.( $DICE_MOD).(EVAL($_self.field_name
))
undo end
!!!!!!!!!!!!!!!!!!!!!!!!!!!!!!!!!!!!!!!!!!!!!!!!!!!!!!!!!!!!!!!!!!!!
entity attributes &
entity_name      = .($DICE_MOD).(EVAL($_self.field_name )) &
type_filter      = Field &
visibility       = no_opinion &
name_visibility  = no_opinion &
&
entity_scope     = all_color &
size             = 1 &
&
transparency     = 0
!!!!!!!!!!!!!!!!!!!!!!!!!!!!!!!!!!!!!!!!!!!!!!!!!!!!!!!!!!!!!!!!!!!!
variable modify variable_name=ip integer_value=(eval(ip+1))
variable modify variable_name=jp integer_value=(eval(jp+1))
variable modify variable_name=kp integer_value=(eval(kp+1))
!
if condition=($LAST_PAR < jp)
break
end
!
! Update the object name strings to new unique values:
variable set variable_name=$_self.field_marker_name
string_value=(UNIQUE_NAME("INT_FIE_MRK"))
variable set variable_name=$_self.field_name
string_value=(UNIQUE_NAME("INT_FIE"))
variable set variable_name=$_self.REF_name
string_value=(UNIQUE_NAME("REF_MAR"))
!
marker create marker=.( $DICE_MOD).ground.(EVAL($_self.REF_name)) location
= ($X_CENT),($Y_CENT),($Z_CENT)
orientation=($INI_ANG+(EVAL(kp))*$CELLSIDE), 0.0, 0.0
!
variable modify variable_name=ra
real_value=(( (Eval(DM((EVAL("INT_PAR_"//ip).cm),
(EVAL($_self.REF_name)))))+(Eval(DM((EVAL("INT_PAR_"//jp).cm),
(EVAL($_self.REF_name)))))))/2)
variable modify variable_name=hi
real_value=(( (Eval(DZ((EVAL("INT_PAR_"//ip).cm),
(EVAL($_self.REF_name)),(EVAL($_self.REF_name)))))+(Eval(DZ((EVAL("INT_PAR_"//jp).cm),
(EVAL($_self.REF_name)),(EVAL($_self.REF_name)))))))/2)
!
!
end ! for

```



## Macro\_contacts

```
!$DICE_MOD:T=Model
!$DICE_PAR:T=part
!$DICE_GEO:T=geometry
!$DICE_GEOS:T=string
!$START_PAR:T=Integer
!$LAST_PAR:T=Integer
!
!!! The DICE_MOD, DICE_PAR, DICE_GEO, and DICE_GEOS variables are the
model, part
!!! and geomtry name of the object to be connected to the multibody
mensicus by
!!! contact elements.  START_PAR and LAST_PAR are the meniscus part's
numeric
!!! suffixes corresponding to the first and last part in the range of
parts to be
!!! connected.
!
!
!
!!! note:the geos string should be the same as the geo variable
variable create variable_name=ip integer_value=$START_PAR
variable create variable_name=$_self.marker_name
string_Value=(UNIQUE_NAME("INT_MRK"))
variable create variable_name=$_self.cylinder_name
string_Value=(UNIQUE_NAME("INT_CYL"))
variable create variable_name=$_self.part_name
string_Value=(UNIQUE_NAME("INT_PAR"))
variable create variable_name=$_self.geo_name
string_Value=(UNIQUE_NAME("INT_GEO"))
variable create variable_name=$_self.csg_name
string_Value=(UNIQUE_NAME("CSG_CELL"))
!
variable create variable_name=$_self.con_f_name
string_Value=(UNIQUE_NAME("CON_F_ELE"))
  variable create variable_name=$_self.gcon_name
string_Value=(UNIQUE_NAME("GCON_FOR"))
!
variable create variable_name=$_self.con_t_name
string_Value=(UNIQUE_NAME("CON_T_ELE"))
  variable create variable_name=$_self.gcon_t_name
string_Value=(UNIQUE_NAME("GCON_T_FOR"))
!
variable create variable_name=$_self.color_flag integer_value=1
variable create variable_name=$_self.color_row_flag integer_value=1
!
!variable create variable_name=$_self.con_f_name
string_Value=(UNIQUE_NAME("CON_F_ELE"))
!
!!!!!!!!!!!!!!!!!!!!!!!!!!!!!!!!!!!!!!!!!!!!!!!!!!!!!!!!!!!!!!!!!!!!!!!!!!!!!!
!!!!!!!!!!!!!!!!!!!!
for variable_name=$_self.r_count start_value=($START_PAR)
increment_value=1 end_value=($LAST_PAR)
!
! Checkerboard colouring: The start colour for each row must alternate:
```

```

    if condition=($_self.color_row_flag==1)
      variable set variable_name=$_self.color_row_flag integer_value=0
    else
      variable set variable_name=$_self.color_row_flag integer_value=1
    end ! if
    variable set variable_name=$_self.color_flag
integer_value=(EVAL($_self.color_row_flag))
!
!
!
!!!!!!!!!!!!!!!!!!!!!!!!!!!!!!!!!!!!!!!!!!!!!!!!!!!!!!!!!!!!!!!!!!!!!!!!!!!!!!!!!!!!!!!!!!!!!!!!!!!!!!!!!!!!!!!!!!!!!!!!
!!!!!!!!!!!!!!!!!!!!!!!!!!!!!!!!!!!!!!!!!!!!!!!!!!!!!!!!!!!!!!!!!!!!!!!!!!!!!!!!!!!!!!!!!!!!!!!!!!!!!!!!!!!!!!!!!!!!!!!!
!!!!!!!!!!!!!!!!!!!!!!!!!!!!!!!!!!!!!!!!!!!!!!!!!!!!!!!!!!!!!!!!!!!!!!!!!!!!!!!!!!!!!!!!!!!!!!!!!!!!!!!!!!!!!!!!!!!!!!!!
!!!!!!!!!!!!!!!!!!!!!!!!!!!!!!!!!!!!!!!!!!!!!!!!!!!!!!!!!!!!!!!!!!!!!!!!!!!!!!!!!!!!!!!!!!!!!!!!!!!!!!!!!!!!!!!!!!!!!!!!
!color objects
!!!!!!!!!!!!!!!!!!!!!!!!!!!!!!!!!!!!!!!!!!!!!!!!!!!!!!!!!!!!!!!!!!!!!!!!!!!!!!!!!!!!!!!!!!!!!!!!!!!!!!!!!!!!!!!!!!!!!!!!
!!!!!!!!!!!!!!!!!!!!!!!!!!!!!!!!!!!!!!!!!!!!!!!!!!!!!!!!!!!!!!!!!!!!!!!!!!!!!!!!!!!!!!!!!!!!!!!!!!!!!!!!!!!!!!!!!!!!!!!!
!
!
! Apply 'checkerboard' colour to cell:
    if condition=($_self.color_flag==1)
      variable set variable_name=$_self.color_flag integer_value=0
      if condition=(DB_EXISTS(EVAL("CSG_CELL_"//ip)))
        geometry attributes
geometry_name=$DICE_MOD.(EVAL("INT_PAR_"//ip)).(EVAL("CSG_CELL_"//ip))
color=maize
      end ! if
    else
      variable set variable_name=$_self.color_flag integer_value=1
      if condition=(DB_EXISTS(EVAL("CSG_CELL_"//ip)))
        geometry attributes
geometry_name=$DICE_MOD.(EVAL("INT_PAR_"//ip)).(EVAL("CSG_CELL_"//ip))
color=Blue
      end ! if
    end ! if
!!!!!!!!!!!!!!!!!!!!!!!!!!!!!!!!!!!!!!!!!!!!!!!!!!!!!!!!!!!!!!!!!!!!!!!!!!!!!!!!!!!!!!!!!!!!!!!!!!!!!!!!!!!!!!!!!!!!!!!!
!!!!!!!!!!!!!!!!!!!!!!!!!!!!!!!!!!!!!!!!!!!!!!!!!!!!!!!!!!!!!!!!!!!!!!!!!!!!!!!!!!!!!!!!!!!!!!!!!!!!!!!!!!!!!!!!!!!!!!!!
!!
!
! The following is used to create a contact for each newly made element to
the DICE_PART
    contact create &
    contact_name = .($DICE_MOD).(EVAL($_self.con_f_name)) &
    &
    &
    i_geometry_name = $DICE_GEO &
    j_geometry_name =
$DICE_MOD.(EVAL("INT_PAR_"//ip)).(EVAL("CSG_CELL_"//ip)) &
    &
    &
    &
    stiffness = ($DICE_MOD.DV_Contact_Stiffness) &
    damping = ($DICE_MOD.DV_Contact_Damping) &
    exponent = ($DICE_MOD.DV_Force_Exponent) &
    dmax = ($DICE_MOD.DV_Contact_dmax) &
    &
    &

```

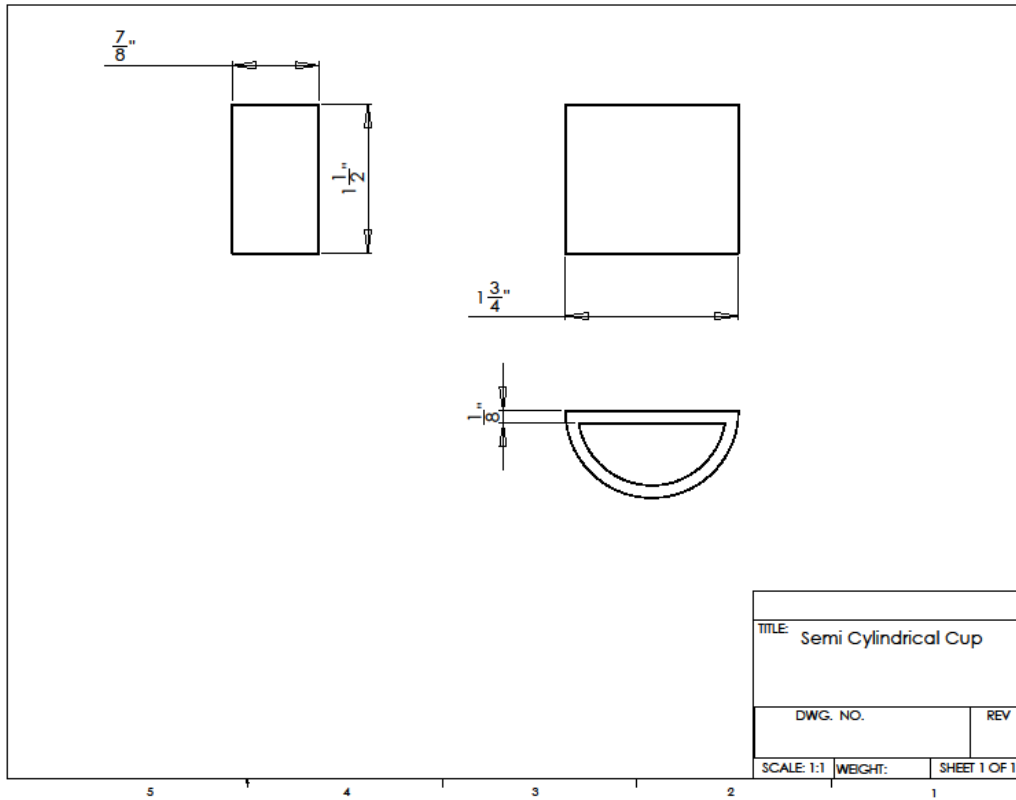
```

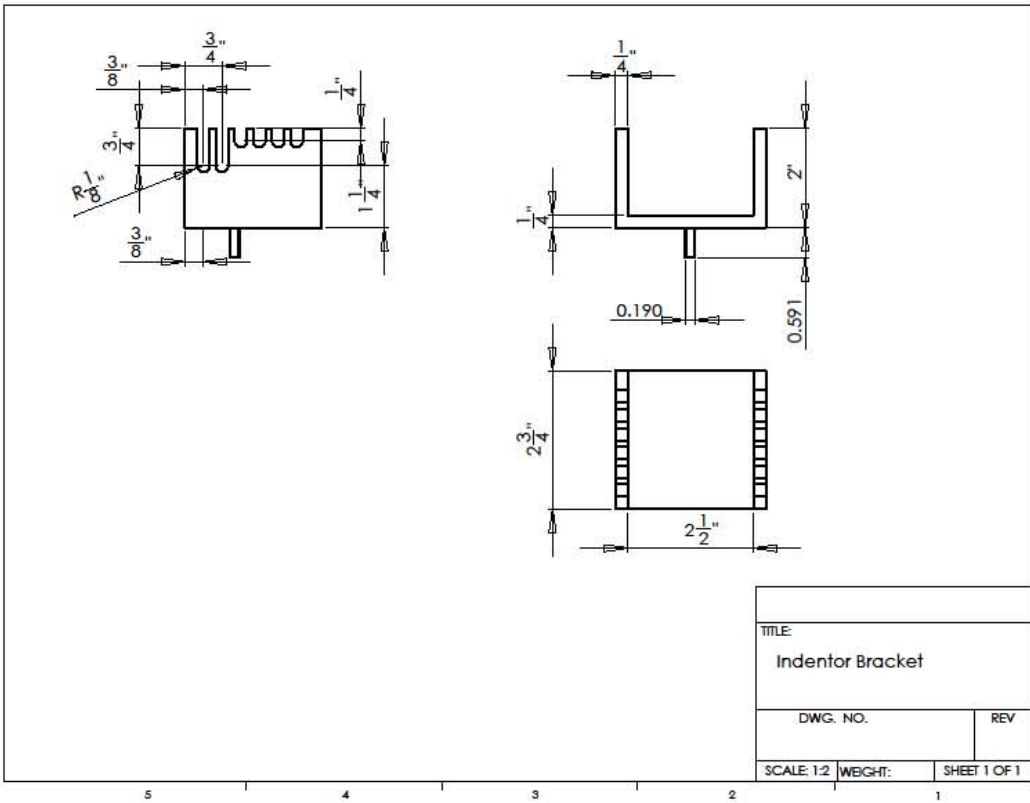
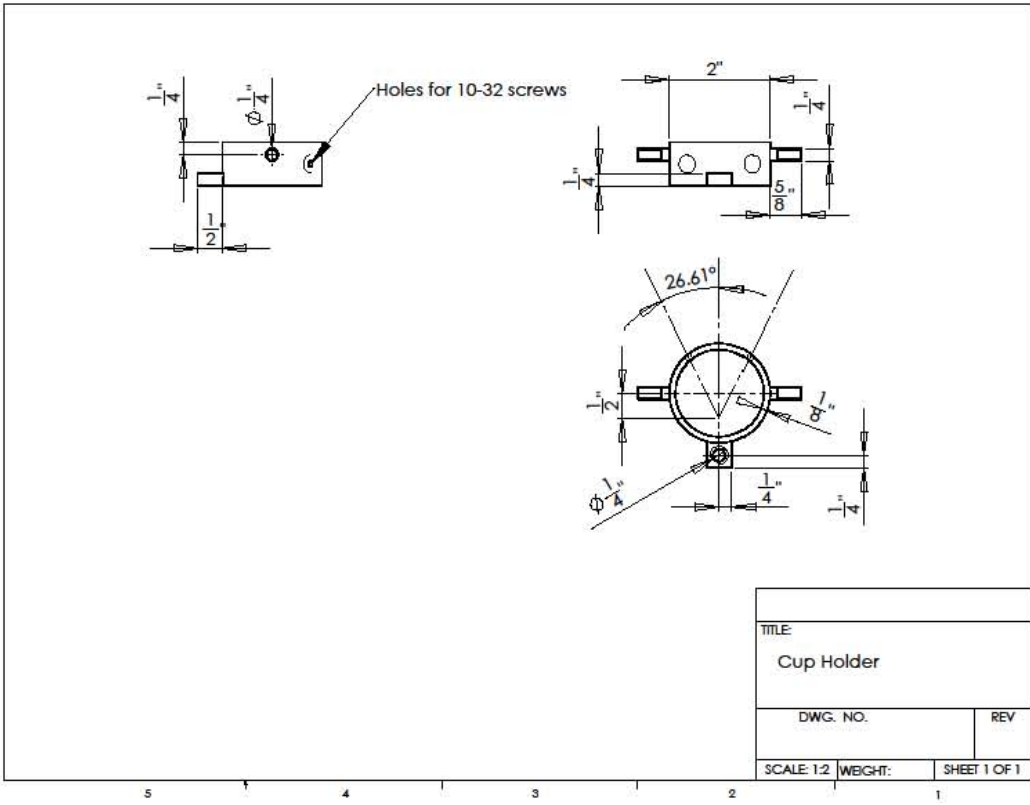
    &
    &
    coulomb_friction = on &
    mu_static = ($DICE_MOD.DV_Contact_MS) &
    mu_dynamic = ($DICE_MOD.DV_Contact_MU) &
    &
    &
    stiction_transition_velocity = ($DICE_MOD.DV_Contact_ST_Vel) &
    friction_transition_velocity = ($DICE_MOD.DV_Contact_FT_Vel)
!!!!!!!!!!!!!!!!!!!!!!!!!!!!!!!!!!!!!!!!!!!!!!!!!!!!!!!!!!!!!!!!!!!!!!!!!!!!
!!!!!!!!!!!!!!!!!!!!!!!!!!!!
!
!!!!!!!!!!!!!!!!!!!!!!!!!!!!!!!!!!!!!!!!!!!!!!!!!!!!!!!!!!!!!!!!!!!!!!!!!!!!
!!!!!!!!!!!!!!!!!!!!!!!!!!!!!!!!!!!!!!!!!!!!!!!!!!!!!!!!!!!!!!!!!!!!!!!!!!!!
!
! Update the object name strings to new unique values:
    variable set variable_name=$_self.marker_name
string_value=(UNIQUE_NAME("INT_MRK"))
    variable set variable_name=$_self.cylinder_name
string_value=(UNIQUE_NAME("INT_CYL"))
    variable set variable_name=$_self.part_name
string_value=(UNIQUE_NAME("INT_PAR"))
    variable set variable_name=$_self.geo_name
string_value=(UNIQUE_NAME("INT_GEO"))
    variable set variable_name=$_self.csg_name
string_value=(UNIQUE_NAME("CSG_CELL"))
    variable modify variable_name=ip integer_value=(eval(ip+1))
    variable set variable_name=$_self.con_f_name
string_value=(UNIQUE_NAME("CON_F_ELE"))
end ! for
!
!!!!!!!!!!!!!!!!!!!!!!!!!!!!!!!!!!!!!!!!!!!!!!!!!!!!!!!!!!!!!!!!!!!!!!!!!!!!
!!!!!!!!!!!!!!!!!!!!!!!!!!!!
!
!!!!!!!!!!!!!!!!!!!!!!!!!!!!!!!!!!!!!!!!!!!!!!!!!!!!!!!!!!!!!!!!!!!!!!!!!!!!
!!!!!!!!!!!!!!!!!!!!!!!!!!!!
!
defaults attributes icon_visibility="off"
view manage modify render=sshaded

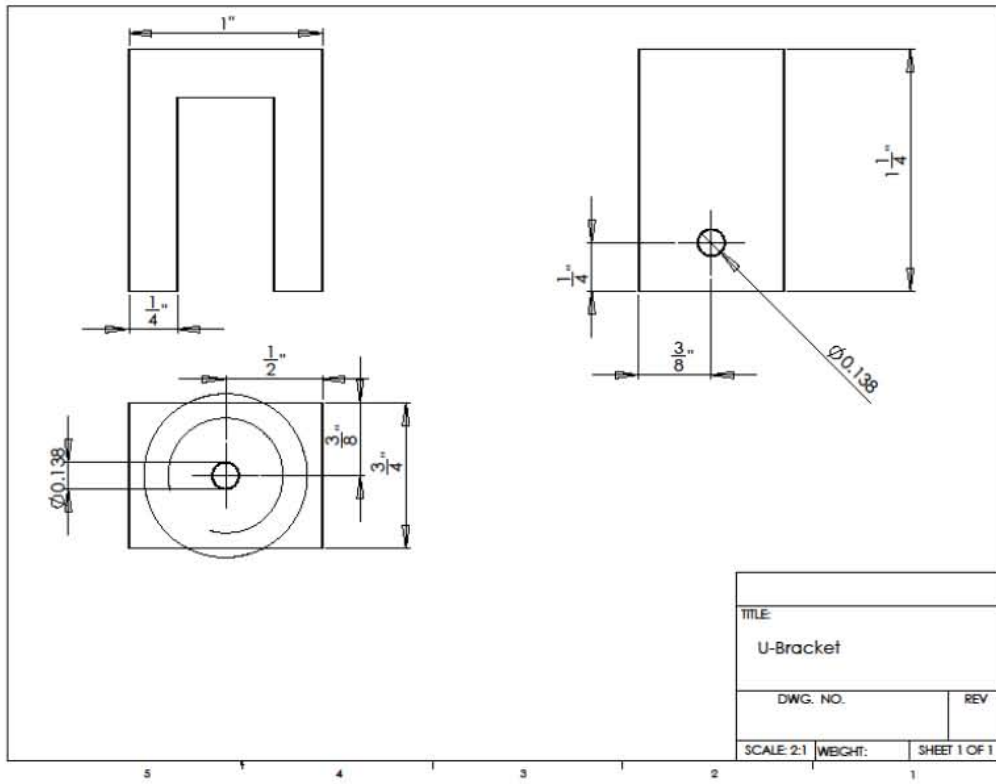
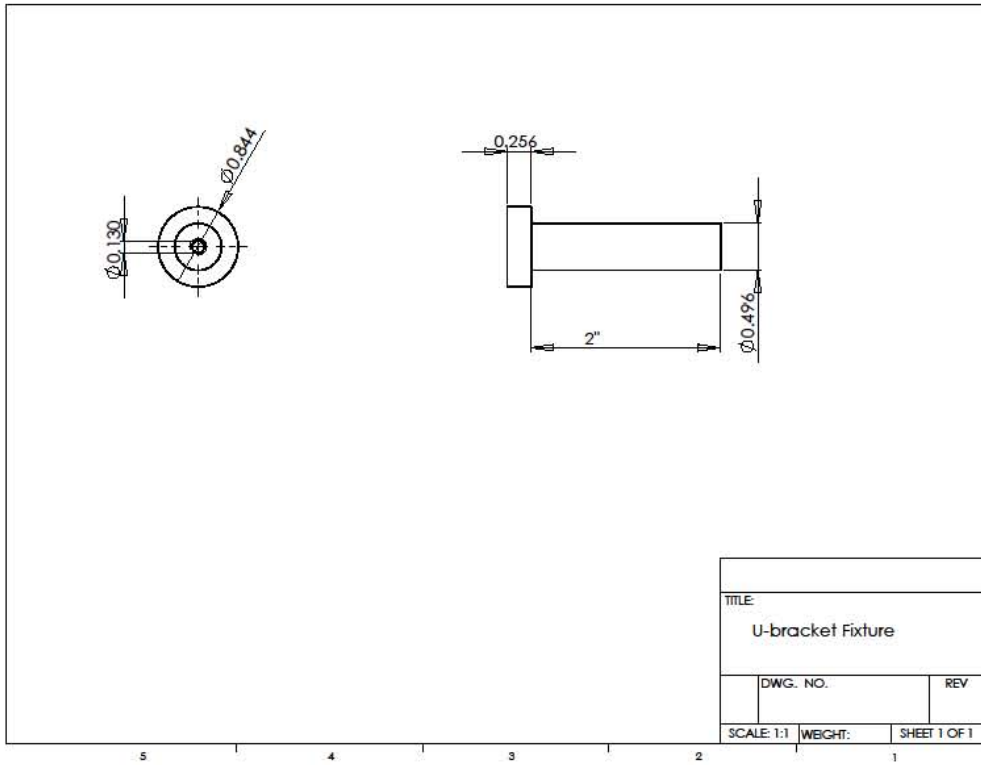
```

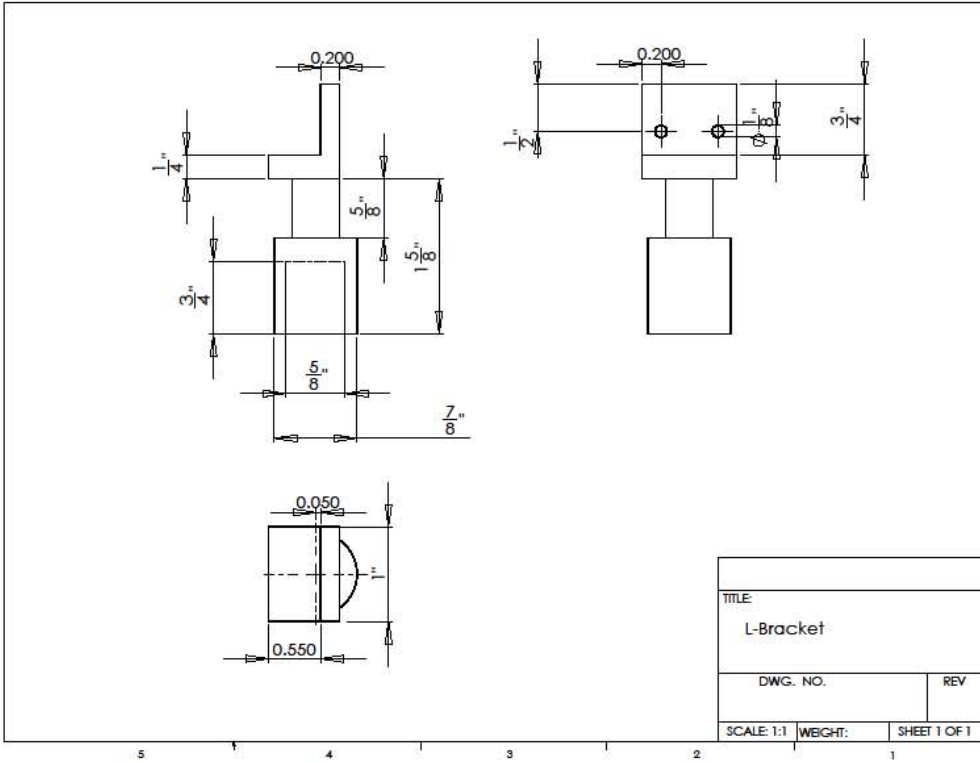
## APPENDIX C

On the following pages are drawing for the fixtures used in this study. They drawings have been resized and are no longer to scale. The first three drawings are of the indentation apparatus and the second three are of the meniscus tester. Not included are drawings of the indenters, v-blocks and the vice plates.









## REFERENCE LIST

- "MD ADAMS 2010 help." [Adams/Solver>C++ Statements>Field](#).
- Chia, H. N. and M. L. Hull (2008). "Compressive Moduli of the Human Medial Meniscus in the Axial and Radial Direction at Equilibrium and at a Physiological Strain Rate." Journal of Orthopedic Research: 951-956.
- Donahue, T. L., M. L. Hull, M. M. Rashid and C. R. Jacobs (2002). "A finite element model of the human knee joint for the study of tibio-femoral contact." J Biomech Eng **124**(3): 273-80.
- Elliott, D. M., R. Jones, 3rd, L. A. Setton, S. P. Scully, T. P. Vail and F. Guilak (2002). "Joint degeneration following meniscal allograft transplantation in a canine model: mechanical properties and semiquantitative histology of articular cartilage." Knee Surg Sports Traumatol Arthrosc **10**(2): 109-18.
- Fithian, D. C., M. K. Kelly and V. C. Mow (1990). "Material Properties and structure-function relationships in the menisci." Clinical Orthopedics and Related Research: 19-31.
- Guess, T. M., G. Thiagarajan, M. Kia and M. Mishra (2010). "A subject specific multibody model of the knee with menisci." Medical Engineering & Physics: 505-515.
- Hayes, W. C., L. M. Keer, G. Herrmann and L. F. Mockros (1972). "A mathematical analysis for indentation tests of articular cartilage." J Biomech **5**(5): 541-51.
- Jurvelin, J. S., J. P. Arokoski, E. B. Hunziker and H. J. Helminen (2000). "Topographical variation of the elastic properties of articular cartilage in the canine knee." J Biomech **33**(6): 669-75.
- McCann, L., E. Ingham, Z. Jin and J. Fisher (2009). "Influence of the meniscus on friction and degradation of cartilage in the natural knee joint." Osteoarthritis Cartilage **17**(8): 995-1000.
- Nigg, B. M. and W. Herzog (1999). Biomechanics of the Musculo-skeletal System. West Sussex, John Wiley & Sons Ltd.
- Pozzi, A., C. A. Tonks and H. Y. Ling (2010). "Femorotibial contact mechanics and meniscal strain after serial meniscectomy." Vet Surg **39**(4): 482-8.
- Shepherd, D. E. and B. B. Seedhom (1997). "A technique for measuring the compressive modulus of articular cartilage under physiological loading rates with preliminary results." Proc Inst Mech Eng H **211**(2): 155-65.
- Sweigart, M. A., C. F. Zhu, D. M. Burt, P. D. DeHoll, C. M. Agrawal, T. O. Clanton and K. A. Athanasiou (2004). "Intraspecies and interspecies comparison of the compressive properties of the medial meniscus." Ann Biomed Eng **32**(11): 1569-79.



- Tawhai, M., J. Bischoff, D. Einstein, A. Erdemir, T. Guess and J. Reinbolt (2009). "Multiscale modeling in computational biomechanics." IEEE Eng Med Biol Mag **28**(3): 41-9.
- Yao, J., J. Snibbe, M. Maloney and A. L. Lerner (2006). "Stresses and strains in the medial meniscus of an ACL deficient knee under anterior loading: a finite element analysis with image-based experimental validation." J Biomech Eng **128**(1): 135-41.

## VITA

Gavin Carson Paiva was born on November 27, 1985, in Rocheport, Missouri. After moving to the Kansas City metropolitan area at an early age he attended public schools and graduated from Shawnee Mission East High School in 2004. He was a repeated state medalist in Kansas Science Olympiad competitions.

After receiving academic scholarships to the University of Missouri-Kansas City he began studying mechanical engineering. As an undergraduate he competed as a member of the Human Powered Vehicle Design Team. He also participated in the Missouri Space Grant Consortium and presented on thermodynamic properties of food. He graduated cum laude in 2008 with a Bachelor of Science Degree in Mechanical Engineering and minors in physics and chemistry.

In fall of 2008 he enrolled in the University of Missouri-Kansas City Graduate School and began work as a graduate research assistant in the Musculoskeletal Biomechanics Research Laboratory. He has worked on cooperative projects with the Human Motion Laboratory and the Computational Intelligence and Bio-Identification Technologies Laboratory at UMKC. Upon completion of the requirements for a Master of Science in Mechanical Engineering, Gavin intends to pursue further education in the field.